Observation of Quantum Correlations in Topological Solid-state Setups

SULTHANA BEGUM

Doctor of Philosophy

ASTON UNIVERSITY

April 2021

Observation of Quantum Correlations in Topological Solid-state Setups

Sulthana Begum

Abstract

Topological insulators are electronic materials that behave like an ordinary insulator internally (in the bulk), but have symmetry protected conducting states on the edge-sites or surface. The simplest case of non trivial topology found amongst these materials is the one-dimensional Su-Schreifer-Heeger (SSH) model. We analyse the unique features within the non-interacting SSH model and explicitly define both the edge states and the bound states and give the conditions of their presence. We show that the total number of bound states crucially depend on the scattering amplitudes and their phases.

The sliding Luttinger liquid (SLL) phase can be destroyed by perturbations such as charge-density wave (CDW) and superconducting (SC). We construct an analogue of the SSH model by coupling one-dimensional quantum wires packed in a two-dimensional array, with alternating couplings between wires. We calculate the scaling dimensions of the two most relevant (dangerous) perturbations, CDW and SC interwire couplings. We create a phase diagram and analyse whether nearest-neighbour interactions stabilise or destroy the SLL phase. Finally, we find a stability region for the SLL.

Keywords: Topological insulators, Su-Schreiffer-Heeger model, bound states, scattering amplitudes, Luttinger liquid, renormalization group, charge-density wave, superconductivity.

Acknowledgements

الحمد لله

I'd like to express my deepest thanks to my supervisor, Dr. Igor V. Yurkevich for the exceptional guidance and mentor-ship that he has provided throughout my time at Aston. I have been incredibly fortunate to have a consistently patient supervisor who encouraged learning above all else. Thank you to Prof. David Saad for being incredibly kind and supporting me with the administration side of this PhD. I'd also like to thank my colleague and collaborator Dr. Adam Lowe for his insights and our many stimulating discussions, in addition to Prof. Victor Flueurov and Prof. Victor Kagalovsky for all of their insights in Chapter 10.

Thank you to my parents who I will forever be indebted to for giving me the opportunity for education. This journey would not have been possible if not for their personal sacrifices, and I dedicate this milestone to them. Special thanks to my brother Habib for his unparalleled kindness, support and willingness to hear about my research for hours during our road-trips. I'm especially grateful to my sister Asma for her unwavering presence in my life and shaping the way that I think with her exceptional analysis of fictional characters in films/books that we shared growing up. Not to forget my other precious sisters; Monwara, Rabeya, Anowara and Hafiza who inspire me every day with their wholehearted kindness and grace.

Finally, my deep and sincere gratitude to all of my wonderful friends for their continuous love and support. Javeria, Aqsa, Humaira, Milly, Jamilah, Safina and Roza, I'd be lost without each one of you and everything you bring to my life. Thank you to my fellow PhD students at Aston for being such a kind and inspirational community that made this experience all the more memorable. Especially my dear friend Reham, who shared all of the ups and downs of this journey and always knew exactly what to say. You kept me sane, thank you.

Contents

List of Figures

Chapter 1

Introduction

Condensed-matter physics is often applied to understand how order emerges in the case of a large number of simple constituents, such as ions or electrons and how they interact with each other. In a crystal, which is an example of an ordered phase, the order can be described through symmetry breaking. The lattice structure of a crystal contains ions that are periodically arranged due to their electrostatic interactions, and therefore, only if you move by an integer number of spacing you return to the same place. Otherwise, the continuous symmetry of space under translations is broken and similarly for rotation.

Topological materials have become of interest since the 1980s [1] with the discovery that electrons confined to two dimensions and subject to a strong magnetic field demonstrate an unexpected type of order. This order is due to the topology of the material and underlies the quantum Hall effect. The outcome is the possibility of dissipation-less transport and the emergent of particles with fractional charge. It has also be discovered that topological order can exist in three-dimensional materials in which the role of the magnetic field is assumed by spin–orbit coupling, an innate property of all solids [2]. We now refer to these materials as topological insulators due to their insulating properties in the bulk and exotic metallic states on their surfaces, or edges. If the edge states [3] for an insulator is found to exist, it is identified as a topological insulator. The metallic surface states originate from topological

invariants [60], which are unique numbers that categorise objects and cannot change as long as a material remains insulating.

Topology [4] is a branch of mathematics that is concerned with objects that are invariant (do not change) under smooth deformations. A classic everyday example being a doughnut transforming into a coffee cup. From a topological perspective, these two objects are the same since the topological invariant (in this case the number of 'holes') is the same. An intuitive illustration displaying why the metallic surfaces exist in topological insulators is shown in Fig. 1.1 To represent a topological insulator we have a trefoil knot and a closed loop is used to represent an ordinary insulator [5],[6]. The knot and the loop have different topological invariants and therefore there are no deformations that would make one become the other. This includes stretching or twisting the string/wire, without cutting it which is not considered a deformation. This is in clear contrast to the doughnut/coffee cup situation. The component of the trefoil knot that is 'knotted' is considered to be the electron's wavefunction as it moves through momentum space. This knotting is associated with a topological invariant which is robust as long as the material remains insulating.

Figure 1.1: Topological insulator represented by a trefoil knot (left) and ordinary insulator represented by a closed loop (right).

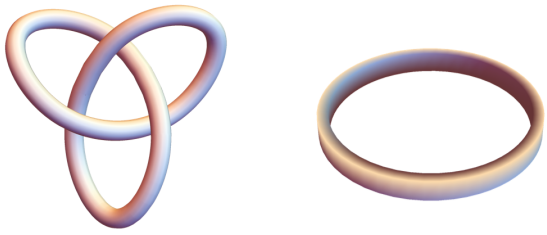

The simplest non-trivial topological model is the Su-Schreiffer-Heeger, or SSH model [8], where each alternating site on the lattice is identical. This model is based on the organic polymer Polyacetylene [9]. In this thesis, we study multiple applications of this model. We begin by identifying the basic distinguishing feature of the model - its topological invariant. We consider a chain of dimers where each dimer (unit cell) contains two different atoms. It

has been found that the topological invariant, Zak-phase [10], which measures the resulting angle formed when Bloch wave-functions travel around a closed loop once, can determine the existence of edge states. This was due to the fact that the Zak-phase was found to control the number of bulk states. In this paper, the authors graphically demonstrated that there were two missing bulk solutions when the ratio between hopping parameters t_1/t_2 was less than the critical ratio $(t_1/t_2)_c = 1 - 1/M + 1$ where M is the number of dimers in the chain. They concluded that in the large M limit, the number of bulk states was related to the value of the Zak-phase ϕ_k at $k = \pi$, since this is the value of wave-number k at which missing states appeared. The missing states were considered to be edge states localised at the ends of the chain and were implicitly found once the boundary condition that the wave-function should disappear at the nearest site outside the chain, at $m = M + 1$ (where m denotes the lattice dimer) was imposed. Edge states could only be solved for in the large M limit when the localisation length was much smaller than the size of the chain. In this limit, the energy of the edge states was found to approach zero.

Figure 1.2: Infinite chain of the polymer Polyacetylene.

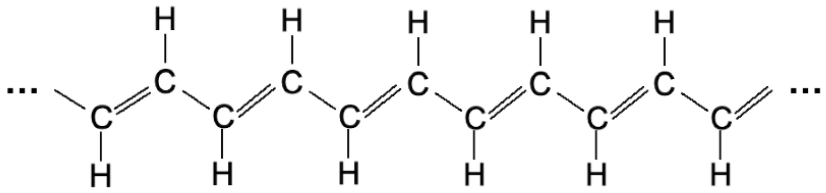

The paper described above considered a chain of dimers which in total has an even number of sites. We aim to explicitly derive the edge states of an odd number of sites in the lattice. An explicit expression describing the edge states will demonstrate the topological nature of the SSH model. Ideally, no such limits should need to be taken to observe edge states, and therefore, we aim to find a universal solution.

Another popular area of interest regarding topological materials and their special states

is the existence of bound states. This is another unique topological protected characteristic that can be observed using the SSH model. Bound states occur when a particle's energy is lower than the potential, in which case the particle cannot escape the potential well and rocks back and forth between the turning points. It is commonly discussed that the Chern number may be used to determine the topological nature of a material. The Chern number [34] is the two-dimensional take on the one-dimensional Zak-phase and measures the adiabatic evolution of an electron confined to some energy band. It is a topological invariant and therefore can be used to identify the topological nature of a material. We propose an alternative approach to extract the same information of a material via scattering amplitudes [15]-[20]. We predict that features of the scattering amplitudes, such as singularities, may contain an indication of topological behaviour. We aim to find the conditions for the existence of bound states [35], how many can exist and if possible, explicitly derive them. The one-dimensional Levinson's theorem [21] can be used to determine the number of bound states and this can be supported by the sum rule. We also aim to check whether the number of bound states is always an integer, and if so, we aim to prove the conditions of this.

We also study interacting systems as opposed to the non-interaction scenarios described above. We consider a 2D system of parallel quantum wires constructed in analogy of the SSH model. In a one-dimensional lattice, the SSH model is constructed such that each alternating site is identical with two different hopping parameters, t_o and t_e. We consider a two-dimensional system of parallel quantum wires coupled with alternating gaps between each wire, g_o and g_e. A Luttinger liquid model [22]-[24] can be used to describe the electronic interaction in each quantum wire which is essentially a one-dimensional conductor. The motivation for introducing this is to serve as a replacement for Fermi liquid theory [25]-[28] which fails in one dimension. In Fermi liquid theory, electronic movement can be described to be 'cloud-like' since multiple electrons move in unison dragging one another forward. This cannot be seen in one-dimension since electronic movement can only be adequately described by scattering linearly and detached from one another. Therefore, the intra-wire interaction described by

Luttinger liquid theory combined with the inter-wire interaction due to coupling between the wires, the sliding Luttinger liquid phase is constructed.

The SLL [29],[30] phase is when all degrees of freedom in a system, such as spin and charge, have zero expectation and their fluctuations are described by power law correlation functions. In a non-SLL phase, some degrees of freedom are frozen and do not fluctuate. We aim to analyse whether nearest-neighbour interwire interactions stabilise or destroy the SLL phase. This can be achieved by calculating analytically the scaling dimensions of the two most relevant interwire perturbations - charge density wave (CDW) and superconductivity (SC) [31],[32]. Charge density wave represents the modulation of conduction electron density coupled with the modulation of lattice atom positions. The modulations are periodic in nature with a wavelength equal to Fermi wavelength λ_F and they produce an energy gap at the Fermi surface at $k = k_F$. The origin of an energy gap in most metal solids is due to the Fourier component of the lattice potential in which electrons move. The origin of energy gap in CDW metals is observed to occur when the modulation wavelength of the position of atoms λ_{atoms} is equal to $2\lambda_F$. As the temperature of CDW metal increases, the electrons easily overcome the energy gap barrier and become normal metals. The CDW phase is an example of a non-SLL phase since there is a non-zero value for some density operators. The superconductive state is observed when certain materials are cooled below their critical temperature resulting in zero resistance. The critical temperature, T_c varies with the individual material. Because these materials have no electrical resistance, meaning electrons can travel freely through them, they can carry large amounts of electrical current for long periods of time without losing energy as heat. We aim to search for a region in which the SLL phase can be stable with both perturbations, CDW and SC being renormalization group, RG [33], irrelevant.

1.1 Thesis Outline

The structure of this thesis is as follows. In chapter 4 we analyse a simple lattice of identical sites. We use the SSH model since it is the simplest non-trivial model to show that the dispersion relation does show an indication of topology. We analyse the hopping parameters t_1 and t_2 and find a critical point at $t_1 = t_2$. The Zak-phase is also calculated and is shown to coincide with this result since $\phi = 2\pi$ when $\nu = 1$ and 0 otherwise. In the same section, edge states for a chain with an odd number of sites are found. The edge states show that when $t_1 < t_2$, the edge state is exponentially localised at the left boundary, and if $t_1 > t_2$ the edge state is exponentially localised at the right boundary instead. Chapter 5 continues the discussion of the SSH model where we derive the scattering amplitudes of waves reflecting off a potential centred on an infinite SSH chain. We do this first for a one-dimensional continuous chain with a δ-function potential. We define λ as the amplitude to the δ-function potential and find that the sign of λ determines the presence of the bound state. We find the bound state and its presence is supported by applying the one-dimensional Levinson's theorem.

Chapters 6 and 7 focus on calculating the density of states using the scattering matrix and the continuity equation. The aim is to determine the number of bound states in the case of nearest-neighbour hopping and once the sum rule is applied, we explicitly show that the number of bound states depends on the reflection amplitude and the phase of the transmission amplitude. We repeat these processes in chapters 8 and 9for the SSH model, and demonstrate that the number of bound states is explicitly an integer. We do this initially for a semi-infinite system and then an infinite system, and study the universality demonstrated in the expression giving the number of bound states.

Finally, we conclude with chapter 10 in which we investigate the stability conditions of the sliding Luttinger liquid phase in a 2D system of parallel quantum wires with alternating coupling between nearest neighbour wires. We analyse the charge-density wave and super-

conducting perturbations with respect to their affect on the stability of the SLL phase. We present an analytical derivation of the CDW and SC scaling dimensions and choose the most dangerous of the scaling dimensions to analyse for each case. We find the stability region of the SLL phase with respect to a Luttinger parameter, a relative coupling strength parameter and a modulation strength parameter. This is done numerically with several plots illustrating the stability region.

Chapter 2

Non-interacting model

2.1 Topology and the Topological band theory of solids

Topology [7] is a geometrical notion used to categorise objects according to the properties that are preserved through deformations. An object that does not change under continuous deformations (or homeomorphisms) like stretching, bending and twisting (not including tearing and sticking) is said to be topological. A very well known example is the case of a coffee-cup and doughnut. Since both have the same number of holes - one, they are considered to be topologically the same object. A pretzel on the other hand has three holes and regardless of hard you try, you can never produce a pretzel from a coffee-cup/doughnut since you'd have to tear two new holes - which breaks a fundamental rule of topology. Therefore, the coffee-cup/doughnut and pretzel each have a unique and robust hole number which is described as the topological invariant, and can be used to categorise the object. This is demonstrated in Fig. 2.1 We have since found that the topological invariant is not restricted to everyday objects, but can also categorise phases of matter [23].

The band theory of solids [36] is one of the greatest achievements of quantum mechanics discovered in the 20th century and arises when the free electron model fails. The free electron model is the simplest way to demonstrate the electronic structure possessed by metals. Although it can be deemed as an oversimplification of the reality, it still is able to describe many

Figure 2.1: Torus with topological invariants (left to right) 0, 1 and 2

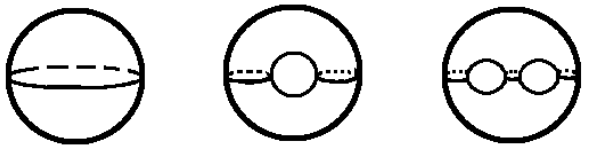

significant properties of metals. The model states that the valence electrons within atoms of the crystal become conduction electrons and are able to move freely and independently of one another through the crystal. The model relies on the assumption of constant potential energy through the solid implying that there are no forces.

Figure 2.2: The periodic potential used to model electrons in a conductor where each ion is the source of a Coulomb potential.

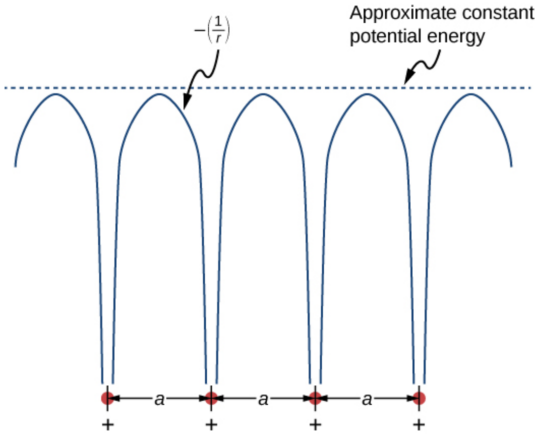

Fig. 2.2 demonstrates that a constant potential energy (dotted line) is not completely representative of the periodic Coulomb potential which behaves as $-1/r$ at each lattice point, where r is the distance between ions and a the distance between atoms. This results in a weakness in the model although the model can still work since on average the potential energy is constant. Secondly, the model also assumes an impenetrable barrier at the surface. This conflicts with results from experiments such as the photoelectric effect [37] where we observe electrons escaping the surface under certain conditions. Moreover, the model consists of several other gaps in explaining the differences in electrical properties of materials such as conductors, semiconductors and insulators. As a result, to compensate for the inadequacies

of the free electron model, the band theory of solids has been introduced as a more complete model.

To introduce band theory we first discuss the covalent bond. The description of the energy structure within a covalent bond begins with two hydrogen atoms spatially separated such that interaction is zero. The electron in each of the hydrogen atoms is in the same ground state. The two atoms are then brought closer together such that the wave functions for each atom overlaps with the other. However, due the exclusion principle [38] the electrons can no longer remain in the same state and therefore, the original energy level is split into two different energy levels which depend on the distance between the atoms. We can introduce more atoms, i.e. four hydrogen atoms brought closer together will form four different energy levels etc. This is demonstrated in Fig. 2.2 where we can see a symmetrical 'hump' between each atom. In the limit of a large number of atoms N, we can expect multiple energy levels forming an energy band shown in Fig.2.3.

Figure 2.3: Demonstration of the formation of energy levels due to the distance between (a) two atoms, (b) four atoms and (c) N atoms.

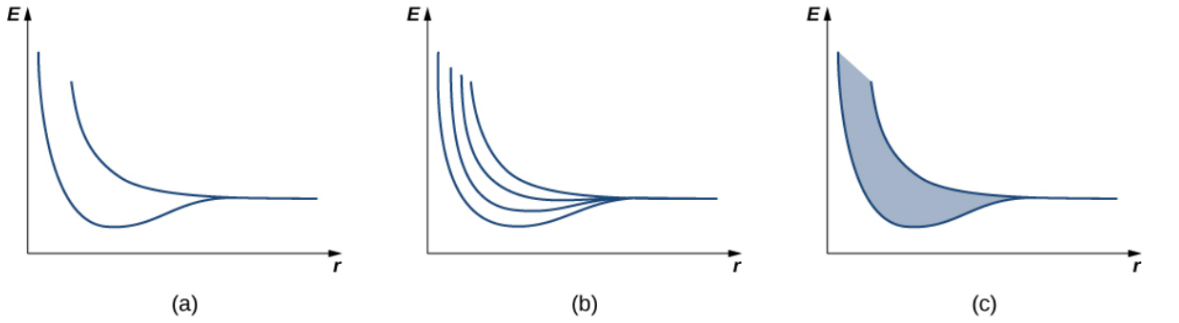

Different energy bands are formed due to the different amount of electrons held in each energy level. Energy bands can be separated from one and another by energy gaps. The concepts of energy bands and energy gaps can explain the differences in electrical properties between conductors and insulators. In a conductor, the conduction band (the available band after the highest energy band is filled) is only partially filled allowing more energy to be oc-

cupied. On the contrary, the conduction band of an insulator is completely filled allowing no room for added energy.

When the interaction between atoms is strong enough for covalent bonding it can lead to crystals forming. When a crystal is formed, band theory can classify the electronic states of the crystal by using the special feature of translational symmetry. The translational symmetry of the electronic states enables us to classify them in terms of their crystal momentum k, defined in a periodic Brillouin zone [39] in reciprocal space. The Bloch states $|U_k\rangle$, defined in a single unit cell of the crystal, are eigenstates of the Bloch Hamiltonian $H(k)$. The eigenvalues ε_k define the energies that collectively form the band structure. An insulating band structure has an energy gap separating the highest occupied band from the lowest empty band. Lattice translation symmetries implies $H(k+G) = H(k)$ for reciprocal lattice vectors G. The crystal momentum is therefore defined in the periodic Brillioun zone, with $k = k + G$. Thus, an insulating band structure can be viewed as a mapping from the Brillioun zone to the space of Bloch Hamiltonians with an energy gap.

2.2 The Hall effect

The motion of charge carriers in magnetic fields has led to many practical discoveries. A magnetic field can be used to deflect an electron beam allowing us to measure the charge to mass ratio of the electrons and ions. This is the concept behind the widely used Mass spectrometer [40] which is used to measure the masses of isotopes, with applications in chemistry, archaeology, planetary science and geology. It is found that the period of orbital motion of any charged particle in a uniform magnetic field is completely independent of the particle's velocity. This concept is the basis for cyclotrons and other particle accelerators, in which high energy collisions are analysed by capturing the curved trajectories of charged particles in magnetic fields.

2.3 The Classical Hall effect

The classical Hall effect [41], or simply, the Hall effect occurs when an electric current flows through a conductor with an applied magnetic field. It has been commonly used to measure the number density and drift velocities of charge carriers in conductors, the latter being in the case of a uniform electric field. The electric field can simply be set up by connecting the terminals of a battery to the conductor. The classical Hall effect has been widely used in magnetic field sensors which are accurate and inexpensive.

A particle with charge q moving with velocity v in a uniform magnetic field B will experience a force F;

$$F = q(v \times B). \tag{2.1}$$

Without an electric field, free electrons in a conducting material (at room temperature) will move in random directions. They will obey a characteristic velocity distribution with an average velocity of zero. An electric field E can be applied by connecting the conductor to a battery and the electrons will accelerate opposite to the field. The electrons can collide with the lattice ions within the conductor slowing them down from the increase in kinetic energy due to the field. The electrons will then acquire a drift velocity, v_d on top of their random velocity. When the magnetic field is applied to a moving charge carrier (such as electrons) within a conductor, a transverse force is exerted on them pushing them to one side. This results in a build-up of opposite charge on the other side of the conductor to balance the magnetic influence. This produces a measurable transverse voltage between the two sides of the conductor and is know as the Hall effect, after E. H. Hall who discovered it in 1879. The Hall voltage is given by;

$$V_H = \frac{IB}{ned}, \tag{2.2}$$

where I is the current, B is the magnetic field, n is the density of moving charge carriers, e is the electron charge and d is the width of the conductor. The transverse resistance (or Hall

resistance), defined as V_H/I is proportional to B/n. This allows the Hall effect to be used to quantify charge carrier type (electron or hole), density and mobilities of electronic materials.

When the charges pile up on either side of the conductor, the force due to the electrostatic field increases until it is balanced by the force due to the magnetic field. This can be expressed as;

$$qE = qv_dB. \tag{2.3}$$

Then the electrostatic field is,

$$E = \frac{V_H}{d}, \tag{2.4}$$

which gives the drift velocity,

$$v_d = \frac{V_H}{Bd}. \tag{2.5}$$

Therefore, it is possible to obtain the drift velocity by measuring the Hall voltage and the magnetic field.

The Hall effect is considered a conduction phenomenon due to the fact that it is different for different charge carriers. The Hall voltage has demonstrated to have different polarities for positive and negative charge carriers. This has led to the study of conduction within semiconductors and other materials that show both positive and negative charge carriers. A Hall probe, which is a thin film placed in between two magnetic pole pieces, can be used to calculate the transverse voltage. The average drift velocity of the moving charge carriers can be measured by moving the Hall probe at varying speeds until the Hall voltage vanishes, showing that the charge carriers are now moving irrespective of the magnetic field.

2.4 The Quantum Hall effect

The quantum Hall effect [11]-[14] is a phenomenon demonstrated when electrons are restricted in a two-dimensional plane with a strong magnetic field. The result of this set-up is that a

conducting material with defects or impurities will behave as it does without the defects under these circumstances. It is necessary to distinguish between two different types of quantum Hall effects that are associated to two related phenomena. They are the integer and fractional quantum Hall effects. The Hall conductivity (ratio of current-voltage) takes quantised values and is defined as;

$$\sigma_{xy} = \frac{e^2}{2\pi\hbar}\nu. \tag{2.6}$$

ν is a topological invariant that is later recognised as one of the most fundamental numbers in topological phases of matter, the Chern number. It is defined by the integral of the Berry curvature over the 2D Brillouin zone, and therefore has close relation to the Berry phase [42],[43]. The Chern number can interpreted as a winding number since it can be multiplied by 2π to obtain the Berry phase.

2.4.1 The integer quantum Hall effect

The integer quantum Hall effect is what is conventionally simply referred to as the quantum Hall effect as it was the first observation of such a phenomenon. We can define the term "conductivity" as the degree to which a specified material conducts electricity, calculated as the ratio of the current density in the material to the electric field which causes the flow of current. Thus, we can define the term 'resistivity' as the inverse of conductivity. In the presence of a magnetic field, the conductivity of a system, σ is given as the matrix,

$$\sigma = \begin{pmatrix} \sigma_{xx} & \sigma_{xy} \\ -\sigma_{xy} & \sigma_{xx} \end{pmatrix}, \tag{2.7}$$

and therefore, the resistivity, ρ is

$$\rho = \sigma^{-1} = \begin{pmatrix} \rho_{xx} & \rho_{xy} \\ -\rho_{xy} & \rho_{xx} \end{pmatrix}. \tag{2.8}$$

As described above, the system focuses on transverse voltage allowing us to focus our

attention on the transverse resistivity, given by ρ_{xy}. The Hall resistivity is given as,

$$\rho_{xy} = \frac{2\pi\hbar}{e^2}\frac{1}{\nu}, \tag{2.9}$$

where $\nu \in \mathbb{Z}$. The first experiments on this topic were constructed in 1980 by von Klitzing [44], taking samples from Dorda and Pepper [45].

Figure 2.4: The integer quantum Hall effect performed by Klitzing, 1980

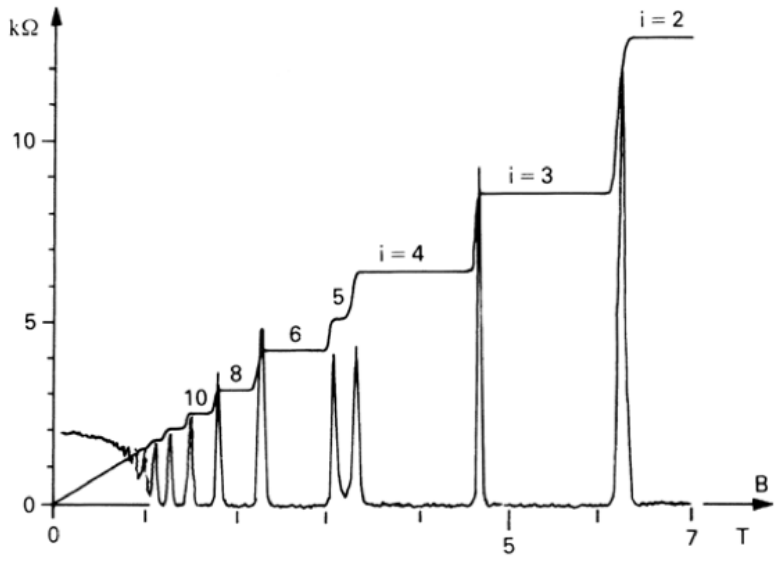

.

The unique feature of the integer quantum Hall effect is that ρ_{xy} remains on a plateau for a range of magnetic field strength, before jumping suddenly to the next plateau. The value of ν is measured to be an integer to a surprising accuracy. The quantity $2\pi\hbar/e^2$ is the 'quantum of resistivity', or the von Klitzing constant, and has since been used as the standard for measuring resistivity.

These plateaux occur when the magnetic field takes the value

$$B = \frac{2\pi\hbar n}{\nu e} = \frac{n}{\nu}\Phi_0 \tag{2.10}$$

where n is the electron density and $\Phi_0 = 2\pi\hbar/e$ is the flux quantum. It was found that the plateaus exist with the quantisation persisting over a range of magnetic fields. Moreover, it was found that the plateaux also persist in the present of disorder, or impurities. This is surprising since impurities usually hinder the understanding of the underlying physics of a system, yet, in the quantum Hall effect, as disorder increases the plateaux become more prominent rather than less. The fact that ν is such a robust property in the sense that it remains consistent despite disorder, we can refer to it as a topological invariant. Whilst we have a plateaux in resistivity, we simultaneously have a plateaux in conductivity. This means that we have finite, well defined conductivity despite disorder. The conductivity lies on the surface with the bulk being insulating, which brings us to topological insulators with conducting edge states.

2.4.2 The fractional quantum Hall effect

In the case of the integer quantum Hall effect, by decreasing the disorder we can observe less prominent plateaux. However, we can also observe other plateaux emerging but at fractional values rather than integer. This was found by Tsui and Stormer in 1982 [47] using samples by Gossard [46]. The resistivities are shown in Fig. 2.5.

Here we observe that the Hall resistivity takes the same form as before, with ν now a rational number, $\nu \in \mathbb{Q}$. Some of the more noticeable plateaux occur for $\nu = 1/3$ and $2/5$. These plateaux emerge more and more with the decrease of disorder. Therefore, it seems likely that in the limit of a perfectly pure sample, we would get an infinite number of plateaux. The would be illustrated with a straight line for the resistivity as expected in the classical Hall effect, in which we expect the transverse resistivity to increase linearly with the magnetic field, B. The fractional quantum Hall requires the we take account the electron-electron interaction rather than the free electron picture as used in the integer quantum Hall effect. This makes the problem more complex and richer. The fundamental ideas were suggested by Laughlin [48], but the topic has been further expanded in many different directions.

Figure 2.5: The fractional quantum Hall effect performed by Tsui and Stormer, 1982

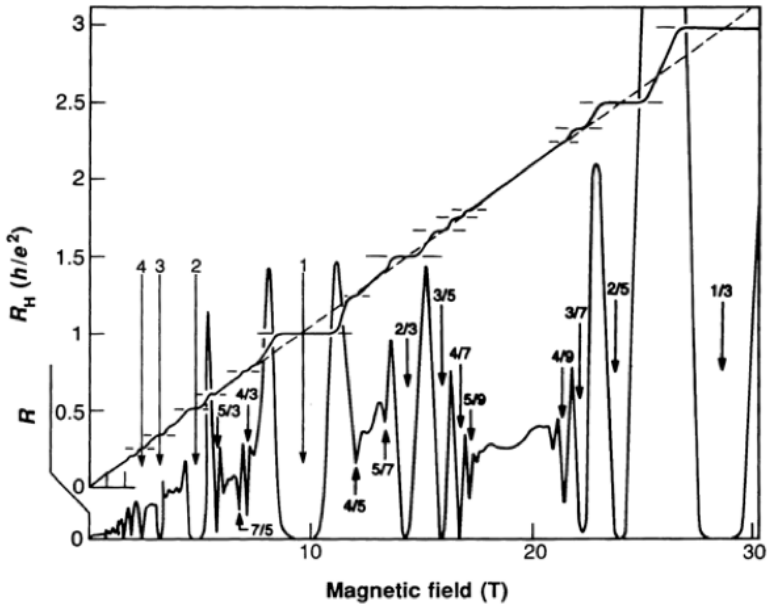

2.5 Topological Insulators

The previous chapters have paved the way for a more detailed discussion of topological insulators which we will do in this section. Topological insulators are a new state of quantum matter with an insulating bulk but with surfaces that can conduct electric current. This behaviour can be described by band theory which says that in the bulk, the Fermi level lies within the conduction and valence bands. This means that there is an energy gap between the ground and first excited states of electrons restricting their movement. However, the electronic states on the surface lie within the bulk energy gap and allow conduction, since the electrons can move and hence conduct charge.

Unlike other materials where the fragile surface states can be changed by details in the surface geometry and chemistry, topological insulators are instead predicted to have unusually robust surface states due to the protection of time-reversal symmetry [50]. These unique states are protected against all time-reversal-invariant perturbations, such as scattering by

Figure 2.6: The valence band and conduction band of a topological insulator.

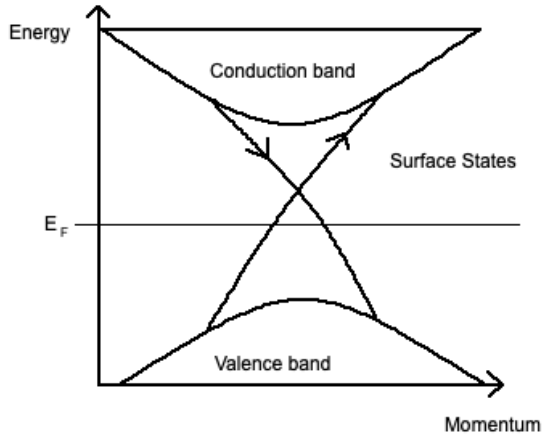

non-magnetic impurities, crystalline defects, and distortion of the surface itself, and can lead to striking quantum phenomena such as quantum spin Hall effect [49]. The robustness of these properties can revolutionise materials and their applications, such as highly efficient nano wires or the basis for storing stable bits in a computer. Extracting the electronic and structural properties of topological insulators is necessary for both understanding the underlying physics and the potential applications. We discuss this further in the next section where we describe a unique topological property, the Berry phase.

2.5.1 Berry/Zak phase and Berry curvature

A Berry phase is a phase angle (between 0 and 2π) that describes how a global phase accumulates as a complex vector is carried around a closed loop in its vector space. Since we are only interested in phases, we can take these complex vectors to be unit vectors, and we will typically identify them with the ground state wave-function of some quantum system. We then consider a gradual change that returns the system to its origin at the end of the loop. This is sketched in Fig. 2.7, where each state $|u_n\rangle$ beginning at $|u_0\rangle$ is projected onto the next state until a loop is formed and the system returns to $|u_N\rangle$.

Figure 2.7: Sketch illustrating states being projected onto each other in ascending order until a loop is formed.

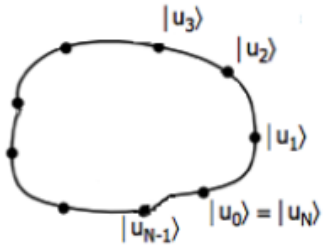

.

The Berry phase ϕ is then defined to be;

$$\phi = -i \ln \langle u_0|u_1\rangle \langle u_1|u_2\rangle \ldots \langle u_{N-1}|u_0\rangle \tag{2.11}$$

$$= -i \ln \prod_{i=0}^{N-1} \langle u_i|u_{i+1}\rangle \,. \tag{2.12}$$

Taylor expanding and defining λ as a continuous real variable that can take on values of N brings us to the result;

$$\phi = -i \oint d\lambda \, \langle u_\lambda|\partial_\lambda u_\lambda\rangle \,. \tag{2.13}$$

Thus, the Berry phase ϕ is minus the complex phase of the product of inner products of the state vectors at neighbouring points around the loop. The integrand in Eq. (2.13) is known as the Berry connection [51], A_λ given as;

$$A_\lambda = i \, \langle u_\lambda|\partial_\lambda u_\lambda\rangle \,. \tag{2.14}$$

When A_λ is integrated in one dimension, we obtain the one-dimensional Berry-phase called the Zak-phase. The Berry phase itself is not topologically invariant and can take any real value or change continuously. However, when a certain symmetry is imposed and a suitable path is considered, the Berry phase can be quantised and give a topological invariant. This is essential for categorisation of wave-functions.

An important point to note is that the Berry connection is not gauge-invariant. If we make a change to the phase of the wave function, u_λ, i.e.

$$|u_\lambda\rangle \to e^{i\alpha_\lambda} |u_\lambda\rangle , \tag{2.15}$$

where α_λ is a continuous real function, and make this substitution into Eq. (2.14), we obtain;

$$A_\lambda \to A_\lambda + \Delta\alpha_\lambda \tag{2.16}$$

so the Berry connection changes by a gradient. The Berry phase however, is gauge-invariant since the integral of $\Delta\alpha_\lambda$ depends only on the initial and final points of the path, hence for a closed path it is zero.

The Berry curvature Ω_λ is defined as the Berry phase per unit area in two-dimensional parameter space, (x, y). We can obtain it by taking the curl of the Berry connection,

$$\Omega_\lambda = \partial_x A_y - \partial_y A_x. \tag{2.17}$$

Like the Berry phase, the curvature is also gauge invariant which can be shown by applying the same transformation in Eq. (2.15).

2.5.2 Winding Number

Another unique topological feature is the winding number [52] which is an integer representing the number of times a closed curve travels anti-clockwise around a given point in the plane. It depends on the orientation of the curve, and is negative if the curve travels around the point clockwise. In Differential geometry, the winding number is expressed as a line integral of a differentiable curve. The derivative in polar coordinates, can be given in terms of rectangular

coordinates as:

$$d\theta = \frac{xdy - ydx}{x^2 + y^2}. \tag{2.18}$$

Then by the fundamental theorem of calculus [53], we can use that the net change in θ is equal to the integral of $d\theta$, giving the winding number as:

$$\nu = \frac{1}{2\pi} \oint \frac{xdy - ydx}{x^2 + y^2}. \tag{2.19}$$

2.6 One-dimensional Levinson's theorem

The Levinson's theorem is an important theorem in the non-relativistic quantum scattering theory, giving the relation between the total number of bound states with the phase of the transmission amplitude. The starting point in the derivation of the one-dimensional Levinson's theorem, is the wave equation,

$$-\frac{d^2\psi}{dx^2} + U(x)\psi = p^2\psi, \tag{2.20}$$

with the boundary $\psi(\pm L) = 0$ with distance L much larger than the scale of the real potential, U. We can define a wavenumber P such that for $p \geq P$ the effects of the potential are negligible and the wave-functions behave as those for a system without a potential. We can then count the number of solutions, N with $0 \leq p \leq P$ given by;

$$N_0 = N + n_b, \tag{2.21}$$

where N_0 is the number of states for a system without a potential and n_b is the number of bound states. This shows that the total number of single-particle states is independent of the presence of potential energy in the Schrödinger equation.

The scattering waves incident the left, ψ_L and from the right, ψ_R

$$\psi_L(x \to -\infty) = e^{ipx} + R_L e^{-ipx}, \quad \psi_L(x \to +\infty) = T_L e^{ipx} \tag{2.22}$$

$$\psi_R(x \to -\infty) = T_R e^{-ipx}, \quad \psi_R(x \to +\infty) = e^{-ipx} + R_R e^{ipx}, \tag{2.23}$$

where R and T are reflection and transmission amplitudes respectively. To define them uniquely, the convention that $p \geq 0$ must be applied. Considering the Wronskians $W(a, b) = ab' - a'b$, we find that $W(\psi_L, \psi_R)$ at $x \to \pm\infty$ leads to

$$T_L = T_R \equiv T. \tag{2.24}$$

Similarly, $W(\psi_L, \psi_R^*)$ leads to

$$\frac{R_L}{R_R^*} = -\frac{T}{T^*}. \tag{2.25}$$

The conservation of flux imposes that

$$|T|^2 + |R_L|^2 = 1 = |T|^2 + |R_R|^2. \tag{2.26}$$

If U is symmetric, $U(x) = U(-x)$, then $W(\psi_L(x), \psi_R(-x))$ leads to

$$R_L = R_R \equiv R. \tag{2.27}$$

The asymptotic conditions for $p \to \infty$ gives

$$T(p \to \infty) = 1 \quad R_L(p \to \infty) = R_R(p \to \infty) = 0. \tag{2.28}$$

At the threshold, $p \to 0$

$$R_L(p \to 0) = R_R(p \to 0) = -1 \quad T(p \to 0) = 0. \tag{2.29}$$

Now we may parametrise T and $R_{L,R}$ accommodating the constraints given above by writing

$$T = \cos\theta e^{i\tau}, \tag{2.30}$$

$$R_L = i\sin\theta e^{i\tau+i\rho}, \tag{2.31}$$

$$R_R = i\sin\theta e^{i\tau-i\rho}, \tag{2.32}$$

with real θ, τ and ρ all functions of p. For symmetric potentials, we have $\rho = 0$. We also adopt the conventions

$$\theta(\infty) = \tau(\infty) = 0, \quad \rho(0) = 0 \tag{2.33}$$

such that

$$-\frac{\pi}{2} < \theta(p) < \frac{\pi}{2}, \quad p > 0, \tag{2.34}$$

and the threshold conditions give:

$$\theta(0) = \pm\frac{1}{2}, \quad \tau(0) = \pi(2\nu \pm \frac{1}{2}), \tag{2.35}$$

where ν is an integer. The aim now is to determine the signs and ν in the equation above in order to determine the phase $\tau(0)$ in terms of bound states of the potential.

We may display the amplitudes T and R in a 2×2 scattering matrix, or S matrix acting on two component vectors (C_L, C_R) whose entries are the coefficients in the expansion of an arbitrary solution $\psi = (C_L\psi_L + C_R\psi_R)$.

$$S = \begin{pmatrix} T & R_R \\ R_L & T \end{pmatrix} \tag{2.36}$$

$$= e^{i\tau}\begin{pmatrix} \cos\theta & ie^{-i\rho}\sin\theta \\ ie^{i\rho}\sin\theta & \cos\theta, \end{pmatrix} \tag{2.37}$$

$$S(\infty) = \begin{pmatrix} 1 & 0 \\ 0 & 1 \end{pmatrix} \quad S(0) = \begin{pmatrix} 0 & -1 \\ -1 & 0 \end{pmatrix}. \tag{2.38}$$

The eigenvalues $S^{1,2}$ for the S matrix and the corresponding eigenvalues $\psi^{1,2}$ are given

$$S^1 = e^{i(\tau+\theta)} \quad S^2 = e^{i(\tau-\theta)}, \tag{2.39}$$

$$\psi^1(x \to \pm\infty) = e^{i(\tau+\theta)/2} \cos\Big[px + \frac{1}{2}(\pm\tau \pm \theta - \rho)\Big], \tag{2.40}$$

$$\psi^2(x \to \pm\infty) = e^{i(\tau-\theta)/2} \sin\Big[px + \frac{1}{2}(\pm\tau \mp \theta - \rho)\Big]. \tag{2.41}$$

We can observe that $\psi^{1,2}$ are real functions of x, which in the case of symmetric potentials and $\rho = 0$, they become the even and odd parity eigenfunctions of S. Therefore, we can drop the norming constants and write

$$\psi^e(x \to \pm\infty) = \cos(px \pm E), \tag{2.42}$$

$$\psi^o(x \to \pm\infty) = \sin(px \pm \Delta), \tag{2.43}$$

where the even and odd parity phase shifts, E and Δ are

$$E(p) = \frac{1}{2}(\tau + \theta), \quad E(\infty) = 0, \quad E(0) = \pi\Big(\nu \pm \frac{1}{2}\Big), \tag{2.44}$$

$$\Delta(p) = \frac{1}{2}(\tau - \theta), \quad \Delta(\infty) = 0, \quad \Delta(0) = \pi\nu. \tag{2.45}$$

2.6.1 Even parity solutions

For states in a system without a potential with $E = 0$ in Eq. (2.44), the boundary conditions $\psi(\pm L) = 0$ imposes the constraint $p_n L = \pi(n + \frac{1}{2})$, with $n = 0, 1, 2\ldots$ Then we can choose $P = \pi(N + \frac{1}{2L})$, which gives the number of states with $0 \le p \le P$ as $N_0^e = (N + 1)$. For systems with a potential with $E \neq 0$ the boundary condition imposes

$$p_n L + E(p_n) = \pi\Big(n + \frac{1}{2}\Big). \tag{2.46}$$

The number of states with $0 \leq p \leq P$ is $N^e = (N - N^e_{min}) + 1$, where n^e_{min} is the lowest possible values of n. Then Eq. (2.21) yields $n^e_b = n^e_{min}$ for the number n^e_b of even parity bound states. We can observe that when $L \to \infty$, p_n with any finite n, hence, p_{min} in particular tends to zero. Thus, we can replace $E(p_n) \to E(0) = \pi(\nu \pm \frac{1}{2})$, which leads to

$$p^e_{min} L = \pi(n^e_{min} + \frac{1}{2} - \nu \mp \frac{1}{2}). \tag{2.47}$$

The asymptotic form of ψ^e ensures that p_{min} cannot be zero since the wave-function would be independent of x, therefore, $p > 0$ and Eq. (2.47) entails $n^e_{min} = (\nu + \frac{1}{2} \pm \frac{1}{2})$, $p_{min} = \pi/L$. Our final results are therefore

$$\nu = n^e_b - \frac{1}{2} \mp \frac{1}{2}, \quad E(0) = \pi(n^e_b - \frac{1}{2}). \tag{2.48}$$

2.6.2 Odd parity solutions

For systems without a potential with $\Delta = 0$ in Eq. (2.43) satisfy $p_n L = \pi n$, $n = 1, 2, 3, \ldots$, so we choose $P = \pi N$. Then the number of states with $0 \leq p \leq P$ is $n^o_0 = N$. Systems with a potential obey

$$p_n L + \Delta(p_n) = \pi n \tag{2.49}$$

and $N^o = (N - n^o_{min} + 1)$ where n^o_{min} and p^o_{min} are the lowest allowed values for each. Then the number n^o_b of odd parity bound states, $n^o_b = N^o_0 - N^o = n^0_{min} - 1$. Then we can replace $\Delta(p_{min})$ by $\Delta(0) = \pi\nu$, which gives

$$p^o_{min} L = \pi(n^o_{min}) - \nu. \tag{2.50}$$

For the same reasons as with the even parity case, we find that $p^o_{min} > 0$, leading to $n^o_{min} = (\nu + 1)$ and $p^o_{min} = \pi/L$. Our final result is therefore

$$\nu = n^o_b, \quad \Delta(0) = \pi n^o_b. \tag{2.51}$$

Collecting our results, we have

$$E(0)/\pi = (\tau(0) + \theta(0))/2\pi = n_b^e - \frac{1}{2} = \nu \pm \frac{1}{2}, \tag{2.52}$$

$$\Delta(0)/\pi = (\tau(0) - \theta(0))/2\pi = n_b^o = \nu. \tag{2.53}$$

For the total number of bound states, we have

$$n_b \equiv n_b^e + n_b^o = 2\nu + \frac{1}{2} \pm \frac{1}{2}. \tag{2.54}$$

Since the upper (lower) signs apply for n_b is odd (even), this implies $n_b^o = n_b^e - 1$ ($n_b^o = n_b^e$). Therefore, our final results are:

n_b is odd:

$$\nu = \frac{1}{2}(n_b - 1), \quad \theta(0) = \frac{1}{2}\pi, \quad \tau(0) = \pi\Big(n_b - \frac{1}{2}\Big); \tag{2.55}$$

n_b is even:

$$\nu = \frac{1}{2}n_b, \quad \theta(0) = -\frac{1}{2}\pi, \quad \tau(0) = \pi\Big(n_b - \frac{1}{2}\Big). \tag{2.56}$$

Chapter 3

Topological aspects in strongly correlated systems

3.1 Fermi Liquid theory

Fermi liquid theory is a model that considers weakly interacting quasi-particles occupying states near the Fermi surface. The Fermi surface is the surface in reciprocal space that separates the fermionic occupied states from unoccupied states at zero temperature. The theory is based on the assumption that near the Fermi surface the gas particles are able to gain energy and weakly interact with one another as liquids.

When particles are added in a non-interacting system, the first particle fills the lowest energy state with each additional particle taking on a higher energy state. If these particles are fermions, the Pauli exclusion principle will ensure that two or more particles cannot occupy the same state. At zero temperature, the level at which states have been occupied is the Fermi level or Fermi energy, ε_F. Then if we introduce temperature, T ($T << \varepsilon_F$) there will be a small probability that the particles will be able to gain energy and jump energy levels. This is only near the Fermi energy as the temperature should not be high enough for particles to jump drastically. Therefore the shift in the particles' energies are by the order of

temperature. The particles in this system are therefore called quasi-particles [54] since they are excited with small energy enabling them to move, collide with and drag other particles along, rather than acting independently.

The rate at which collisions can occur around the Fermi level is given as

$$\frac{1}{\tau} = \alpha\Big(\frac{T}{\varepsilon_F}\Big)^2 \tag{3.1}$$

Here τ is the mean free time which is the average time in between two collisions and α is the coupling constant between two particles which describes how strong the collisions are between particles. Therefore, the LHS is the rate at which particles collide and the RHS describes the scattering of particles from collisions. The restriction that particles can shift in energy, momentum and velocity only around the Fermi level ensures that there are not many particles that are able to be scattered. As a result, the rate of collisions and scattering is low. Therefore, Fermi liquids can be described as non-interacting or weakly interacting particles due to the suppressed scattering between them. In contrast, a Fermi gas has a scattering rate of 0 since in this model there is no interaction. When temperature is increased, a Fermi gas model becomes like a Fermi liquid model due to the increase in scattering, and therefore interaction between electrons. As a result, the cloud-like, or quasi-particle description of electrons is introduced for systems with interaction which would otherwise be simply referred to as a free electron model in the absence of interaction.

Since there are many constraints that need to be satisfied for energy and momentum for multiple interacting particles, this description is not suitable for one-dimension in which there are far fewer constraints due the restriction of dimensionality. In one-dimension, particles can only move linearly and detached from other particles which contrary to the description of 'cloud-like' movement in Fermi liquid theory.

3.2 Renormalization Group Theory

The subject of renormalization group (RG) theory refers to a systematic investigation of the changes a physical system undergoes whilst viewed at different scales. As the scale changes, the system at one scale will be seen to contain self-similar copies of itself when viewed at a smaller scales with different parameters describing the components of the system.

To describe the macroscopic behavior of a physical system that is undergoing an RG transformation, a relevant observable A is required. If the magnitude of A seems to be increasing as the length scale of the system goes from small to large, then A is said to RG relevant. Otherwise, if A appears to be decreasing it is said to be RG irrelevant. The third case in which it neither appears to be increasing or decreasing, it is said to RG marginal.

The process begins with the statistical mechanics of a system described by some Hamiltonian H. Equilibrium properties can then be determined by the partition function

$$Z = \sum_X e^{-\beta H} = \sum_X e^{-S}, \tag{3.2}$$

where X denotes all configurations and the action $S = \beta H$. In general, the action contains degrees of freedom for wavevectors up to some cutoff Λ, which is of the order of the dimensions of the Brillouin zone. The aim is to obtain and 'effective action' containing only the physical most relevant degrees of freedom. In standard phase transition situations, this is the vicinity and the cutoff is defined with respect to this surface. This can be achieved by proceeding as follows:

1. Starting from a cutoff-dependent action $S(\Lambda)$ one eliminates all degrees of freedom between Λ and Λ/s, where s is a scale factor larger than 1. This gives rise to a new action $S'(\Lambda' = \Lambda/s)$.

2. One performs a 'scale change' $k \to sk$. This reinforces the cutoff to its original value and a new action $S'(\Lambda)$ is obtained.

3. One chooses a value of s infinitesimally close to 1: $s = 1+\varepsilon$, where $\varepsilon << 1$, and performs the first two steps iteratively. This then gives rise to differential equations for the couplings which can be integrated until all irrelevant degrees of freedom have been eliminated. This idea of deriving scaling laws to observe only relevant degrees of freedom allows us to reduce a complex interacting system to an effective model described by only a few parameters.

3.3 Luttinger Liquid Theory

A Luttinger liquid is a model describing interacting fermions (more specifically, electrons) in a one-dimensional conductor, such as quantum wires, and is necessary when the Fermi liquid model breaks down. The system is described to be strongly correlated due to the restriction in dimension which increases the probability of interaction. Since particle-hole excitations are bosonic in character, bosonization which is an effective field theory that focuses on low-energy excitations is applied. In this case, Luttinger bosons are considered elementary excitations resulting in density waves, or fluctuations in liquid density.

3.3.1 Bosonization

Much like in the theory of Fermi liquids, we focus our attention only at the vicinity of the Fermi energy since all other regions are irrelevant or unoccupied. The dispersion law can be reduced to two straight lines near points around the Fermi energy. As a result, there can be two branches of particles, one branch of particles moving to the right with momentum q and the other to the left with momentum $-q$. This is a description of the non-interacting model [55],[56]. The Hamiltonian density for the Luttinger model is given as:

$$\mathcal{H} = -iv_F[\psi_R^\dagger \partial_x \psi_R - \psi_L^\dagger \partial_x \psi_L] \tag{3.3}$$

where ψ_R and ψ_L denote states for right moving and left moving particles respectively. We can introduce the density operator to describe the interaction between particles:

$$n_R(x) = \psi_R^\dagger(x)\psi_R(x), \tag{3.4}$$

which obeys the fundamental relation:

$$[n_{R-q}, n_{Rq}] = \frac{qL}{2\pi}. \tag{3.5}$$

This is the commutation relation between the density operator at q and $-q$ and is shown to anti-commute with $\frac{qL}{2\pi}$. Since for bosons the commutation relation is 1, we can re-scale by writing the operators in another way. We introduce the following boson creation and annihilation operators for $q > 0$

$$b_{Rq}^\dagger = (2\pi/qL)^{1/2} n_{Rq} \tag{3.6}$$

$$b_{Rq} = (2\pi/qL)^{1/2} n_{R-q} \tag{3.7}$$

which obey the Bose commutation relations, $[b_{Rq}, b_{Rq}^\dagger] = 1$. Applying these operators to the Hamiltonian gives

$$\mathcal{H}_R = \frac{1}{2\partial n/\partial\mu} \int dx n_R(x)^2 \tag{3.8}$$

in position space, and

$$= \frac{\pi\hbar v_F}{L}\Big[N_R^2 + \sum_{q>0} b_{Rq}^\dagger b_{Rq}\Big] \tag{3.9}$$

in momentum space. It is useful to express the chiral density in terms of a chiral phase operator,

$$n_R(x) = \partial_x \phi_R(x)/(2\pi). \tag{3.10}$$

In terms of ϕ_R the commutation relation Eq. (3.5) becomes:

$$\Big[\frac{\partial_x \phi_R(x)}{2\pi}, \phi_R(x')\Big] = i\delta(x - x'). \tag{3.11}$$

This suggests that $\partial_x \phi_R(x)$ and $\phi_R(x)$ are canonically conjugate variables similar to x and p in fundamental quantum mechanics. This allows us to write the Lagrangian, typically written as $L = p\dot{q} - H(p, q)$, but now as:

$$L = -\frac{1}{4\pi}\partial_x \phi[\partial_t \phi_R + v_F \partial_x \phi_R]. \tag{3.12}$$

Chapter 4

One-dimensional Topological Insulators: The SSH model

The Su-Schreiffer-Heeger model (or simply the SSH) is the simplest model to demonstrate non-trivial topology. An SSH lattice model consists of each alternating site to be identical with two different hopping parameters. Due to its simplicity, it has been applied in literature as a starting point for determining the existence of edge states.

For the SSH every other site of the lattice is identical. To distinguish between the two different sites, we will label them as odd and even. The hopping parameters t_o and t_e represent the probability of a particle moving between these sites. Though the arrangement of hopping parameters and sites is irrelevant initially, once set it is essential that the arrangement is kept consistent for the calculations ahead.

Considering nearest-neighbour hopping only, we can construct a Hamiltonian as:

$$\hat{H} = -t_o \sum_n [\hat{c}^\dagger_{2n-1}\hat{c}_{2n} + \hat{c}^\dagger_{2n}\hat{c}_{2n-1}] - t_e \sum_n [\hat{c}^\dagger_{2n}\hat{c}_{2n+1} + \hat{c}^\dagger_{2n+1}\hat{c}_{2n}] \tag{4.1}$$

Figure 4.1: One-dimensional SSH lattice with alternating identical sites

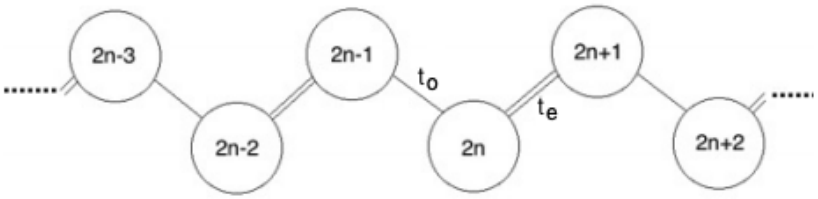

Using the ground state:

$$|\psi\rangle = \sum_j \psi_j \hat{c}_j^\dagger |0\rangle \,, \tag{4.2}$$

we can obtain the wave-functions for odd and even sites as:

$$-t_o\psi_{j-1} - t_e\psi_{j+1} = \varepsilon\psi_j, \quad j = 2n+1 \tag{4.3}$$

$$-t_o\psi_{j+1} - t_e\psi_{j-1} = \varepsilon\psi_j, \quad j = 2n \tag{4.4}$$

Since we have a periodic potential, we can use the Bloch waves to find the eigenenergies ε:

$$\psi_j = e^{ikj}U_k^o, \quad j = 2n+1 \tag{4.5}$$

$$\psi_j = e^{ikj}U_k^e, \quad j = 2n \tag{4.6}$$

then the Schrödinger equation becomes:

$$\hat{H} = \begin{pmatrix} 0 & -t_o e^{ik} - t_e e^{-ik} \\ -t_o e^{-ik} - t_e e^{ik} & 0 \end{pmatrix} \begin{pmatrix} U_k^e \\ U_k^o \end{pmatrix} = \begin{pmatrix} \varepsilon & 0 \\ 0 & \varepsilon \end{pmatrix} \begin{pmatrix} U_k^e \\ U_k^o \end{pmatrix}, \tag{4.7}$$

with eigenenergy

$$\varepsilon_\pm = \pm\sqrt{t_o^2 + t_e^2 + 2t_o t_e \cos 2k}, \tag{4.8}$$

and eigenvectors

$$U_k = \begin{pmatrix} 1 \\ \pm\sqrt{\frac{t_k^*}{t_k}} \end{pmatrix} = \frac{1}{\sqrt{2}} \begin{pmatrix} 1 \\ \pm e^{-i\phi(k)} \end{pmatrix} \tag{4.9}$$

where $t_k = t_o e^{ik} + t_e e^{-ik}$.

The energy bands described in Eq. (4.8) are shown in Fig. 4.2. From this figure, we

Figure 4.2: Energy bands for the SSH model

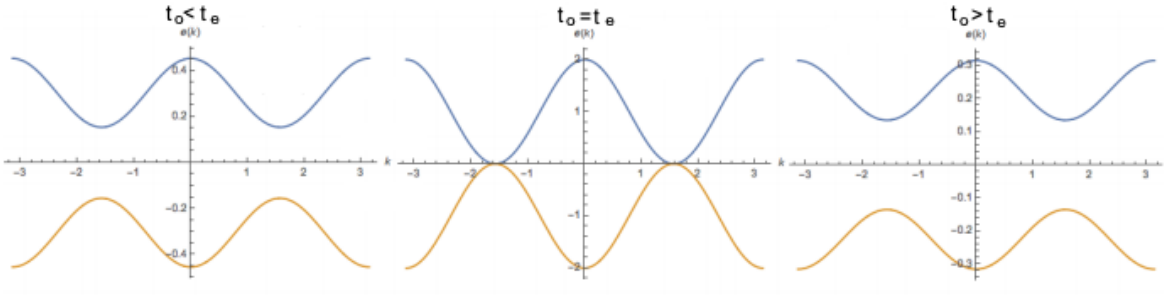

can see that at $t_o = t_e$ the energy bands touch indicating a flow of electrons and therefore, conduction.

4.1 Zak-Phase

We can define the complex number, t_k, as $t_k = |t_k|e^{i\phi(k)}$. The ratio of t_1/t_2 can determine whether t_k circles the origin or not. The Zak-phase, which describes the closed path the particle takes in momentum space, is defined as;

$$Z = i \oint dk \left\langle U_k \middle| \frac{\partial}{\partial k} U_k \right\rangle . \tag{4.10}$$

Substituting the eigenvectors in Eq. (4.9) into Eq. (4.10), we obtain the Zak-phase as;

$$Z = \oint dk \frac{d\phi}{dk} = 0, \pi \tag{4.11}$$

The Zak-phase is π times the winding number of the curve t_k around the origin, and is therefore, zero if the curve does not enclose the origin.

4.2 Winding number

Using the complex logarithm function;

$$ln(t_k) = ln(|t_k|e^{iarg(t_k)}) = \ln|t_k| + iarg(t_k), \tag{4.12}$$

the winding number of the closed contour, t_k around the origin is given as;

$$\nu = \frac{1}{2\pi i}\oint dk \frac{d}{dk}\ln(t_k) \tag{4.13}$$

Substituting $t_k = t_o e^{ik} + t_e e^{-ik}$, we have;

$$\nu = -1 + \frac{1}{2\pi i}\oint dk \frac{e^{2ik}}{t_e/t_o + e^{2ik}} \tag{4.14}$$

Using the substitution $z = e^{2ik}$,

$$\nu = -1 + \frac{1}{2\pi i}\oint \frac{dz}{z + t_e/t_o}. \tag{4.15}$$

To solve this integral, we calculate the residue at $z = -t_e/t_o$;

$$\nu = -1 + \lim_{z\to -\frac{t_e}{t_o}} \frac{z - (-\frac{t_e}{t_o})}{z + \frac{t_e}{t_o}} = 0. \tag{4.16}$$

Therefore, the winding number of t_k is trivially 0 when the point $z = \left|\frac{t_e}{t_o}\right|$ lies inside the unit circle, i.e. $t_o > t_e$, and has the topologically non-trivial value of -1 otherwise ($t_o < t_e$). Since the winding number represents the number of times the vector encircles the origin in the counter-clockwise direction, we will neglect the minus sign. Fig. 4.3 demonstrates the different values for winding number depending on the relationship between t_o and t_e. We can

Figure 4.3: (left to right) topological transition from trivial to non-trivial winding number

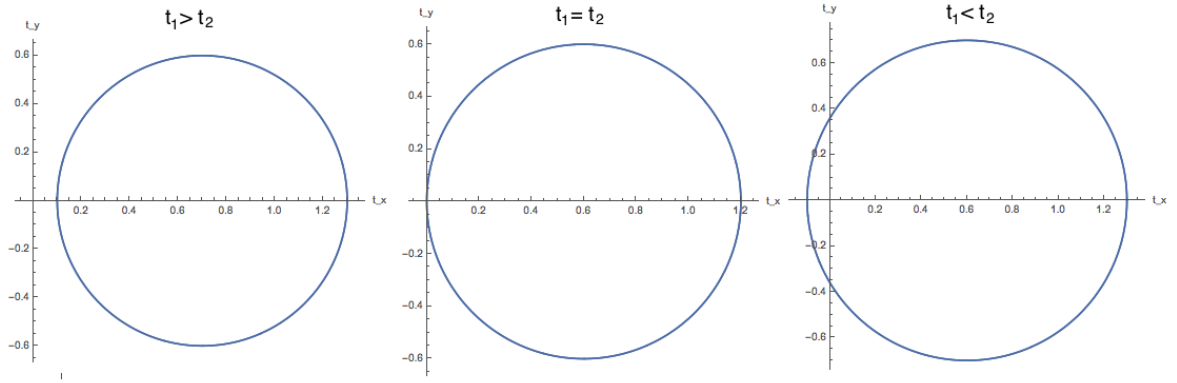

see that when $t_o > t_e$, t_k does not enclose the origin, hence the topologically trivial winding number of 0. On the other hand, when $t_o < t_e$, t_k does enclose the origin, hence the topologically non-trivial winding number of an integer (in this case 1). This transition occurs at $t_o = t_e$ in which t_k only touches the origin. In Fig. 4.2, we saw that when $t_o = t_e$ we have a gap-less state, i.e. the gap between the bands closes, which is an indication of conduction due to topology.

As discussed in the previous section, the Zak-phase is given as 2π times the winding number. Therefore, we can observe that in the trivial case, $Z = 0$, and in the non-trivial case when $\nu = 1$, we have $Z = 2\pi$.

4.3 Bulk states and Edge states

In this section we will derive the bulk states which exist for the finite SSH model. Boundary conditions can be imposed to obtain a lattice of finite sites. By restricting the SSH to a finite lattice of an odd number of sites, we can observe the appearance of edge states.

We can imagine two sub-lattices, one with M even sites only and the other with $M + 1$ odd sites only, resulting in a total of $2M + 1$ sites. We obtained the eigenfunctions in Eq's.

(4.3) and (4.4) where we re-label j as $2j$ to emphasise it is even:

$$t_o\psi_{2j-1} + t_e\psi_{2j+1} = \varepsilon\psi_{2j}, \quad j = 1, ..., M \tag{4.17}$$

$$t_e\psi_{2j-2} + t_o\psi_{2j} = \varepsilon\psi_{2j-1}, \quad j = 1, ..., M+1 \tag{4.18}$$

We can restrict the lattice to a finite system by introducing the boundary conditions such that the wave-function is 0 at sites $j = 0$ and $j = 2M + 2$:

$$\psi_0 = \psi_{2M+2} = 0. \tag{4.19}$$

The eigenfunctions are also labelled by a wave vector, k and can be represented by a linear combination of two plane waves travelling left and right:

$$\psi_{k,2j} = e_k e^{ikj} + e_{-k}e^{-ikj} \tag{4.20}$$

$$\psi_{k,2j-1} = o_k e^{ikj} + o_{-k}e^{-ikj}, \tag{4.21}$$

where the coefficients e_k and o_k are the amplitudes of the waves and satisfy the equations:

$$t_k o_k = \varepsilon_k e_k \tag{4.22}$$

$$\bar{t_k} e_k = \varepsilon_k o_k, \tag{4.23}$$

with $t_k = t_o + t_e e^{ik} = |t_k|e^{i\phi_k}$.

Solving for eigen-energies ε_k we obtain the dispersion describing two bands:

$$\varepsilon_{\pm k} = \pm|t_k|. \tag{4.24}$$

Inserting the boundary condition $\psi(0) = 0$ into Eq. (4.20) we obtain:

$$e_{-k} = -e_k. \tag{4.25}$$

Eq. (4.25) allows us to derive the bulk states:

$$\psi^b_{\pm k,2j} = A_k \sin kj, \tag{4.26}$$

$$\psi^b_{\pm k,2j-1} = \pm A_k \sin(kj - \phi_k), \tag{4.27}$$

Which once normalised, we find:

$$A_k = \frac{1}{\sqrt{M+1}}. \tag{4.28}$$

The second boundary condition $\psi_{2M+2} = 0$ leads to the quantisation of the wave vector:

$$\begin{aligned} \sin k(M+1) &= 0, \\ k = \frac{\pi n}{M+1}, \quad n &= 1, ..., M. \end{aligned} \tag{4.29}$$

This quantisation suggests that there are M solutions in each of the bulk states, resulting in a total of $2M$ bulk solutions labelled by k. However, since we initially began with $2M+1$ degrees of freedom, we can suggest that there is an extra solution at the edge of the lattice - an edge state. An educated guess tells us that we can try to find this edge state by taking $\varepsilon = 0$. One way to solve Eq.'s (4.26) and (4.27) for the edge states, is to take one to be zero, and observe the movement of the wave on the other. In other words, we can set $\psi_{2j} = 0$, and observe only ψ_{2j-1}. Doing so, we obtain:

$$-\frac{t_o}{t_e}\psi_{2j-1} = \psi_{2j+1}. \tag{4.30}$$

The solution to the recurrence relation can be solved to give the edge state as:

$$\psi^e_{2j-1} = N_0\Big(-\frac{t_o}{t_e}\Big)^j, \quad \psi^e_{2j} = 0, \quad N^e = \Big[\frac{(-\frac{t_o}{t_e})^2 - (-\frac{t_o}{t_e})^{2(M+2)}}{1-(-\frac{t_o}{t_e})^2}\Big]^{-1/2}. \tag{4.31}$$

When $t_o < t_e$, the edge state will have a maximum value when $j = 1$ and will exponentially decrease as j increases. Therefore, we can say that the edge state is exponentially localised at the left boundary, and the plane wave will travel from left to right. If $t_o > t_e$, the maximum

value that the edge state can take is at $j = M+1$ which decreases exponentially as j decreases. Therefore, we have the reflected wave instead (travelling right to left) since the edge state will now be exponentially localised at the right boundary.

4.4 Chapter summary

We used the SSH model to demonstrate unique topological behaviour. The topological transition from trivial to non-trivial behaviour is at $t_o = t_e$. We observed that there is an edge state which is localised at the left boundary and occurred when $t_o < t_e$. If this ratio is flipped, the edge state will move to the right boundary.

Chapter 5

Scattering Amplitudes for one-dimensional systems

Topological insulators can exist due to different protected states. In previous chapters, we have discussed topologically protected states due to edge states far from the bulk in the energy gap. There can also be protected states in the bulk due to the nature of a potential which restricts a particle's motion such that it is localised in one region - we call these bound states. In this section we discuss bound states for topologically non-trivial perturbation by calculating reflection/transmission coefficients. As opposed to the conventional route [60] of calculating the Chern number from the Hamiltonian in order to determine the topological nature of a material, we propose another method involving calculating scattering amplitudes to extract the same information. For a one-dimensional model we devise a method to calculate the Zak-phase from the scattering amplitude. We propose a criterion that takes a material and calculates the scattering amplitude allowing us to determine its topologically trivial (or non-trivial) nature.

5.1 Scattering amplitudes for a continuous chain

To begin with, we will develop the protocol of finding bound states by analysing scattering amplitudes for a one-dimensional infinite continuous chain. In this model, the chain will be uniform and identical everywhere, with the exception of a δ-potential in exactly the centre of the chain acting as a barrier for incoming and outgoing waves.To observe scattering states with momentum k, we consider a potential much smaller than the wave-length of the system. As a result, we may choose a delta-function potential since it can be used to approximate the function on the small scale with a relevant coefficient. The Schrödinger equation for the model is;

$$-\frac{d^2}{dx^2}\psi(x) + \lambda\delta(x)\psi(x) = \varepsilon\psi(x), \tag{5.1}$$

where λ is the amplitude of the δ-function potential and ε is the energy of the model. To find scattering amplitudes, more precisely, the reflection coefficient, we will send plane waves e^{ikx} from both left and right hand sides of the chain and observe the scattering behaviour demonstrated. For now, we may consider only incoming waves from the left to simplify calculation. Since waves incoming from the left are identical to waves incoming from the right, the scattering behavior is also identical. Therefore, the scattering states on the left are given by;

$$\psi_L^S(x) = e^{ikx} + r_k e^{-ikx} \tag{5.2}$$

and on the right,

$$\psi_R^S(x) = t_k e^{ikx}, \tag{5.3}$$

where k is the complex wave-vector restricted in the upper half plane ($k = k + i0$)and r_k, t_k are the reflection and transmission coefficients. To solve Eq. (5.1), we impose the following boundary conditions;

$$\psi_L(0) = \psi_R(0), \quad \psi'_R(0) - \psi'_L(0) = -\lambda\psi(0). \tag{5.4}$$

Applying these boundary conditions to Eq.'s (5.2) and (5.3), we obtain,

$$t_k = 1 + r_k, \tag{5.5}$$

$$r_k = -\frac{\lambda}{2ik + \lambda}. \tag{5.6}$$

The standard energy ε for a plane wave solution to the Schrödinger equation is $\varepsilon = k^2$. Therefore the singularity is

$$\lambda = -2ik = -2i\sqrt{\varepsilon}. \tag{5.7}$$

The square root, $\sqrt{\varepsilon}$ can be analytically continued in the upper half plane to give $i\sqrt{\varepsilon}$. Therefore, λ is instead now positive;

$$\lambda = 2\sqrt{\varepsilon}, \tag{5.8}$$

as expected for the potential to take the form of a 'well' as required for a bound state. Therefore, the wave-functions taking the form e^{ikx}, become;

$$\psi_L^B(x) = \sqrt{2}\varepsilon_0^{\frac{1}{4}} e^{-i(i\sqrt{\varepsilon_0})} = \sqrt{2}\varepsilon_0^{\frac{1}{4}} e^{\sqrt{\varepsilon_0}x}, \tag{5.9}$$

$$\psi_R^B(x) = \sqrt{2}\varepsilon_0^{\frac{1}{4}} e^{i(i\sqrt{\varepsilon_0})} = \sqrt{2}\varepsilon_0^{\frac{1}{4}} e^{-\sqrt{\varepsilon_0}x}, \tag{5.10}$$

where ε_0 is the energy of the bound state. We can observe that the wave-functions exponentially decay on either side of the potential. They are localised about the potential, with the highest probability of positioning right next to the potential which then decays to 0 as we move away from the potential.

5.2 Bound states for a continuous chain

We have just seen that bound states may be derived through the scattering amplitudes of a system. However, information about the presence of bound states can also be found through the total charge of the system. This can lead to explicitly quantifying the number of bound states. The total charge at zero temperature is given by;

$$\int_0^{k_F} \frac{dk}{2\pi} \int_{-\infty}^{\infty} dx \left|\psi^S(x)\right|^2 + \int_{-\infty}^{\infty} dx \left|\psi^B(x)\right|^2, \tag{5.11}$$

where k_F is the Fermi momentum and $\psi^S(x)$ and $\psi^B(x)$ are the scattering and bound states respectively.

Inserting our arbitrary scattering and bound states from the previous section and subtracting an unperturbed state e^{ikx} to compensate for any divergent terms, we have

$$\int_0^{k_F} \frac{dk}{2\pi} \Big\{ \int_{-\infty}^{0} dx \Big[1 + |r_k|^2 + \bar{r}_k e^{2ikx} + r_k e^{-2ikx} - \Big| e^{ikx} \Big|^2 \Big] + \int_0^{\infty} dx \Big[|t_k|^2 - \Big| e^{ikx} \Big|^2 \Big] \Big\} + 1, \tag{5.12}$$

since $|t_k|^2 = 1 - |r_k|^2$ using Eq.'s (5.5) and (5.6) and the bound states integrate to give 1. The integral in Eq. (5.12) reduces to;

$$\int_0^{k_F} \frac{dk}{2\pi} \int_{-\infty}^{0} dx 2 \Big[\bar{r}_k e^{2ikx} + r_k e^{-2ikx} \Big] \tag{5.13}$$

Due to symmetry, we are able to combine terms under one integral and have chosen $-\infty$ to 0. We have also now accounted for our earlier simplification of choosing waves only incoming from the left by introducing a factor of 2 such that we have waves incoming from the left and right. Integrating over x, integral becomes;

$$\int_0^{k_F} \frac{dk}{\pi} \Big[\frac{\bar{r}_k}{2i\bar{k}} - \frac{r_k}{2ik} + \lim_{x \to -\infty} \frac{r_k}{2i\bar{k}} e^{-2ikx} \Big]. \tag{5.14}$$

Since $k = k + i0$, the limit goes to zero and we are left with;

$$\frac{\lambda}{2\pi i}\int_0^{k_F} dk\Big[\frac{1}{(k+i0)(2ik+\lambda)}-\frac{1}{(k-i0)(-2ik+\lambda)}\Big]. \tag{5.15}$$

Using the following definition:

$$\frac{1}{k+i0}=P\frac{1}{k}-i\pi\delta(k), \tag{5.16}$$

we have:

$$\frac{\lambda}{2\pi i}\int_0^{k_F} dk\Big[\frac{P}{k}\frac{-4ik}{4k^2+\lambda^2}-i\pi\delta(k)\frac{2\lambda}{4k^2+\lambda^2}\Big] \tag{5.17}$$

for $\lambda > 0$.

Computing the two terms separately, we have:

$$\frac{\lambda}{2\pi i}\int_0^{k_F} dk\Big[\frac{P}{k}\frac{-4ik}{4k^2+\lambda^2}\Big]=\frac{-\lambda}{2\pi}P\int_0^{k_F} dk\frac{1}{(k+i\lambda/2)(k-i\lambda/2)}. \tag{5.18}$$

$$=\frac{-2\lambda}{\pi}\frac{1}{2\lambda}\arctan\frac{2k_F}{\lambda}, \tag{5.19}$$

where we have treated the principal value integral as a regular integral since there are no singularities.

The second term in Eq. (5.17) gives,

$$\int_0^{k_F} dk\frac{-\lambda^2\delta(k)}{4k^2+\lambda^2}=\frac{1}{2}[1-2\theta(k_F)]=\frac{-1}{2} \tag{5.20}$$

since $k_F > 0$. Combining our results, we obtain:

$$\frac{-1}{\pi}\arctan\frac{2k_F}{\lambda}-\frac{1}{2}=\frac{-1}{\pi}\frac{\pi}{2}-\frac{1}{2}=-1, \tag{5.21}$$

in the limit $\lambda \to 0$.

We can finally conclude that in the presence of the bound state which only has the contribution '+1', the total charge is 0 and -1 otherwise.

5.3 Scattering amplitudes for Bravais lattice

We now repeat our steps in section 5.1 for a one-dimensional simple lattice with identical sites j and a repeating hopping amplitude, 1. For simplicity, we begin with particle hopping to nearest-neighbour sites only. To observe the scattering behaviour of this model, we will deform the lattice by placing an impurity, λ at the origin. The Schrödinger equation is:

$$-\frac{1}{2}(\psi_{j+1}+\psi_{j-1}) = (\varepsilon_k - \lambda\delta_{0j})\psi_j, \tag{5.22}$$

where ε_k is the energy with wave vector, k. For lattice sites greater than $j = 1$ and less than $j = -1$, i.e. $|j| \geq 1$, we have:

$$-\frac{1}{2}(\psi_{j+1}+\psi_{j-1}) = \varepsilon_k\psi_j. \tag{5.23}$$

We can seek solutions in the form:

$$\psi_j = ae^{ikj} + be^{-ikj}, \tag{5.24}$$

with arbitrary coefficients, a and b to obtain the bulk energy,

$$\varepsilon_k = -\cos k \tag{5.25}$$

The scattering behaviour around the impurity, λ can be given by the following three wave-functions;

$$(\varepsilon_k - \lambda)\psi_0 = -\frac{1}{2}(\psi_1 + \psi_{-1}), \tag{5.26}$$

$$\varepsilon_k\psi_1 = -\frac{1}{2}(\psi_0 + \psi_2), \tag{5.27}$$

$$\varepsilon_k\psi_{-1} = -\frac{1}{2}(\psi_0 + \psi_{-2}). \tag{5.28}$$

Using the definitions:

$$\psi_{j\geq 1} = t_k e^{ikj}, \tag{5.29}$$

$$\psi_{j\leq -1} = e^{ikj} + r_k e^{-ikj}, \tag{5.30}$$

where t_k and r_k are the transmission and reflection amplitudes respectively, we obtain the relations:

$$\psi_0 = t_k = 1 + r_k, \qquad r_k = \frac{-\lambda}{\lambda - i\sin k}, \qquad t_k = \frac{\sin k}{\sin k + i\lambda} \tag{5.31}$$

To find bound states, we can observe that r_k has poles at the following:

$$\lambda = i\sin k_0 \qquad \text{for } \lambda > 0, \tag{5.32}$$

$$\lambda = -i\sin k_0 \qquad \text{for } \lambda < 0. \tag{5.33}$$

Therefore, we find the wave-vector of the bound state, k_0 with the corresponding energy, ε_0 and bound states:

for $\lambda > 0$,

$$k_0 = \arcsin(-i\lambda) = \pi + i\,\mathrm{arcsinh}\,\lambda \tag{5.34}$$

$$\varepsilon_0 = \sqrt{1+\lambda^2} \tag{5.35}$$

$$\psi_R = e^{ik_0 j} = e^{i(\pi + i\,\mathrm{arcsinh}\,\lambda)j} = (-1)^j e^{-\,\mathrm{arcsinh}\,\lambda j} \tag{5.36}$$

$$\psi_L = e^{-ik_0 j} = e^{-i(\pi + i\,\mathrm{arcsinh}\,\lambda)j} = (-1)^j e^{\mathrm{arcsinh}\,\lambda j} \tag{5.37}$$

For $\lambda < 0$,

$$k_0 = i\,\mathrm{arcsinh}\,\lambda \tag{5.38}$$

Figure 5.1: The wavefunction for $\lambda > 0$ represents scattering states oscillating around the impurity and then behaving as free-particles at $\pm\infty$.

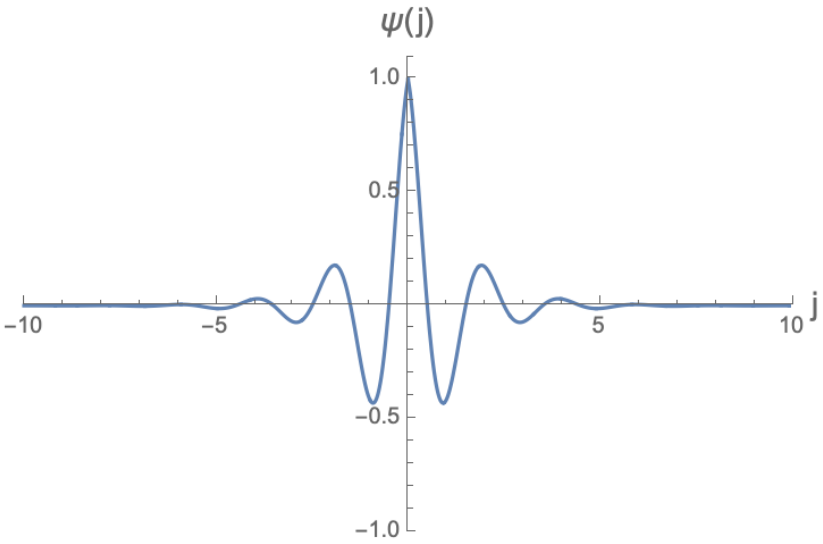

$$\varepsilon_0 = -\sqrt{1+\lambda^2} \tag{5.39}$$

$$\psi_R = e^{ik_0 j} = e^{i(i\,\mathrm{arcsinh}\,\lambda)j} = e^{-\,\mathrm{arcsinh}\,\lambda j} \tag{5.40}$$

$$\psi_L = e^{-ik_0 j} = e^{-i(\mathrm{arcsinh}\,\lambda)j} = e^{\mathrm{arcsinh}\,\lambda j}. \tag{5.41}$$

The phase of the transmission amplitude, $\tau(k)$ is given as:

$$\tau_k = \arctan\frac{\lambda}{\sin k} \tag{5.42}$$

which in the $\lim_{k\to 0}$, $\tau(0) = \pi/2$.

Applying the one-dimensional Levinson's theorem which states that:

$$\tau(0) = \pi\Big(n_b - \frac{1}{2}\Big), \tag{5.43}$$

Figure 5.2: The wavefunction for $\lambda < 0$ is the bound state that we are looking for. It is shown to be localised about the centre and then exponentially decaying far from the origin.

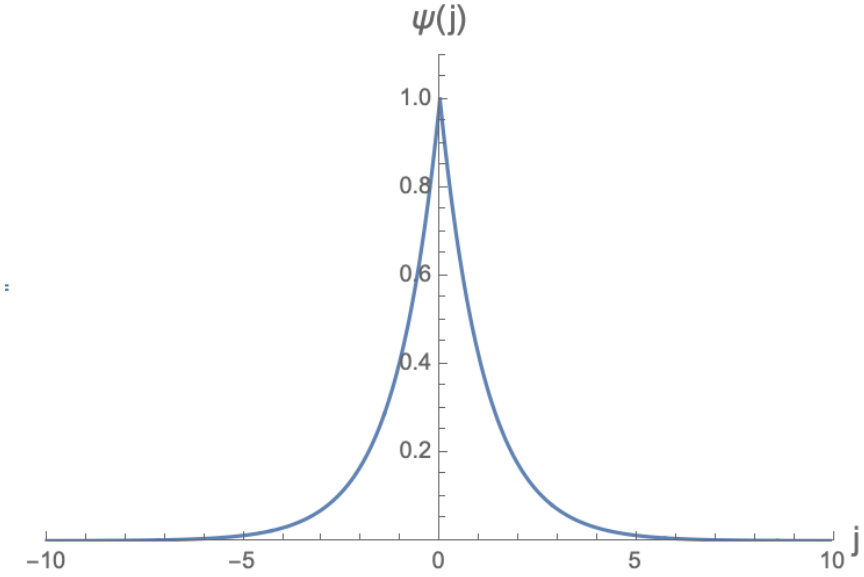

where n_b is the number of bound states, gives:

$$n_b = \frac{\tau(0)}{\pi} + \frac{1}{2} = 1, \tag{5.44}$$

which coincides with our result in section 5.1 where we also found one bound state. We can see here that tuning the parameter λ leads to the band-gap either closing/opening, and therefore, the absence/presence of the bound state. For $\lambda < 0$ the bound state is present and it is absent otherwise.

5.4 Scattering amplitudes for the SSH Model

In this section, we will implement the procedure devised in the previous section on the SSH Model. However, we will slightly alter the model by inserting an impurity, such as the delta function, in the centre of the chain, $j = 0$. We imagine two sub-lattices, A and B, which define the wave-function:

$$\psi_j = \begin{pmatrix} A_j \\ B_j \end{pmatrix} \tag{5.45}$$

.

As before, we consider nearest-neighbour hopping only, therefore, the Schrödinger equations for lattice sites with hopping amplitudes τ_1 and τ_2 at $j \leq -1$ are given:

$$\begin{aligned} -\varepsilon A_j &= \tau_1 B_{j-1} + \tau_2 B_j \\ -\varepsilon B_j &= \tau_2 A_j + \tau_1 A_{j+1}, \end{aligned} \tag{5.46}$$

and for $j \geq 1$:

$$\begin{aligned} -\varepsilon A_j &= \tau_2 B_j + \tau_1 B_{j+1} \\ -\varepsilon B_j &= \tau_1 A_{j-1} + \tau_2 A_j, \end{aligned} \tag{5.47}$$

and for $j = 0$:

$$-\varepsilon A_0 = \tau_1 (B_1 + B_{-1}). \tag{5.48}$$

The bulk waves, $|j| \geq 1$ can be defined as plane waves, $\psi_j = U_k e^{ikj}$ with wave vector, k. This gives, for $j \leq 1$,

$$\begin{pmatrix} \varepsilon_k & \bar{\tau_k} \\ \tau_k & \varepsilon_k \end{pmatrix} U_k = 0, \tag{5.49}$$

and for $j \geq 1$,

$$\begin{pmatrix} \varepsilon_k & \tau_k \\ \bar{\tau_k} & \varepsilon_k \end{pmatrix} U_k = 0, \tag{5.50}$$

where,

$$\varepsilon_k^2 = |\tau|^2 = \tau_1^2 + \tau_2^2 + 2\tau_1\tau_2 \cos k, \tag{5.51}$$

$$\tau = \tau_2 + \tau_1 e^{ik}. \tag{5.52}$$

Then solving for eigen-functions, U_k, we obtain the wave-functions:

$$\psi_{j\leq 1}(\varepsilon_k) = \alpha \begin{pmatrix} \varepsilon_k \\ -\tau \end{pmatrix} e^{ikj} + \beta \begin{pmatrix} \varepsilon_k \\ -\bar{\tau} \end{pmatrix} e^{-ikj} \tag{5.53}$$

and

$$\psi_{j\geq 1}(\varepsilon_k) = \gamma \begin{pmatrix} \varepsilon_k \\ -\bar{\tau} \end{pmatrix} e^{ikj} + \delta \begin{pmatrix} \varepsilon_k \\ -\tau \end{pmatrix} e^{-ikj} \tag{5.54}$$

with coefficients α, β, γ and δ. Since normalisation ensures that the amplitude of the incoming waves should be 1, and we are interested in scattering behaviour of the wave-functions due to the δ-function potential, we have

$$\psi_{j\leq 1}(\varepsilon_k) = \begin{pmatrix} \varepsilon_k \\ -\tau \end{pmatrix} e^{ikj} + r_k \begin{pmatrix} \varepsilon_k \\ -\bar{\tau} \end{pmatrix} e^{-ikj} \tag{5.55}$$

and

$$\psi_{j\geq 1}(\varepsilon_k) = t_k \begin{pmatrix} \varepsilon_k \\ -\bar{\tau} \end{pmatrix}, \tag{5.56}$$

where r_k and t_k are the reflection and transmission amplitudes respectively.
To derive r_k and t_k , we first define wave-functions nearest to the impurity.

$$\begin{aligned} A_1 &= t_k \varepsilon_k e^{ik} \\ B_1 &= -t_k \bar{\tau}_k e^{ik} \\ A_{-1} &= \varepsilon_k (e^{-ik} + r_k e^{ik}) \\ B_{-1} &= -\tau_k e^{-ik} - r_k \bar{\tau}_k e^{ik}, \end{aligned} \tag{5.57}$$

which can be reduced to:

$$\begin{aligned} -\varepsilon_k B_{-1} &= \tau_2 A_{-1} + \tau_1 A_0 \\ -\varepsilon_k B_1 &= \tau_2 A_1 + \tau_1 A_0 \\ -\varepsilon_k A_0 &= \tau_1 (B_1 + B_{-1}). \end{aligned} \tag{5.58}$$

Finally, we obtain:

$$t_k = \frac{A_0}{\varepsilon_k} = 1 + r_k \tag{5.59}$$

and

$$r_k = -\frac{\tau_2^2 - \tau_1^2}{\tau_2^2 - \tau_1^2 - 2i\tau_1\tau_2 \sin k} = -\frac{1-\tau^2}{(1-\tau e^{ik})(1+\tau e^{-ik})}, \tag{5.60}$$

where the RHS is obtained by defining $\tau = \tau_1/\tau_2$. Then

$$t_k = \frac{2\tau \sin k}{2\tau \sin k + i(1-\tau^2)}. \tag{5.61}$$

Analysing the poles in the upper imaginary plane for the reflection amplitude, we find for $\tau < 1$

$$\tau = -e^{ik_0}, \quad k_0 = \pi - i \ln \tau, \tag{5.62}$$

$$\varepsilon_0 \equiv \varepsilon(k_0) = 0 \tag{5.63}$$

$$\psi_R = e^{ik_0 j} = e^{i(\pi - i\ln\tau)j} = (-1)^j e^{\ln\tau j}, \tag{5.64}$$

$$\psi_L = e^{-ik_0 j} = e^{-i(\pi - i\ln\tau)j} = (-1)^j e^{-\ln\tau j}. \tag{5.65}$$

and for $\tau > 1$,

$$\tau = e^{-ik_0}, \quad k_0 = i \ln \tau, \tag{5.66}$$

$$\varepsilon_0^2 = 2\tau_2^2(1+\tau^2). \tag{5.67}$$

$$\psi_R = e^{ik_0 j} = e^{i(i\ln\tau)j} = e^{-\ln\tau j}, \tag{5.68}$$

Figure 5.3: The wavefunction for $\tau < 1$ is the scattering state oscillating about the origin and fading to zero at $\pm\infty$.

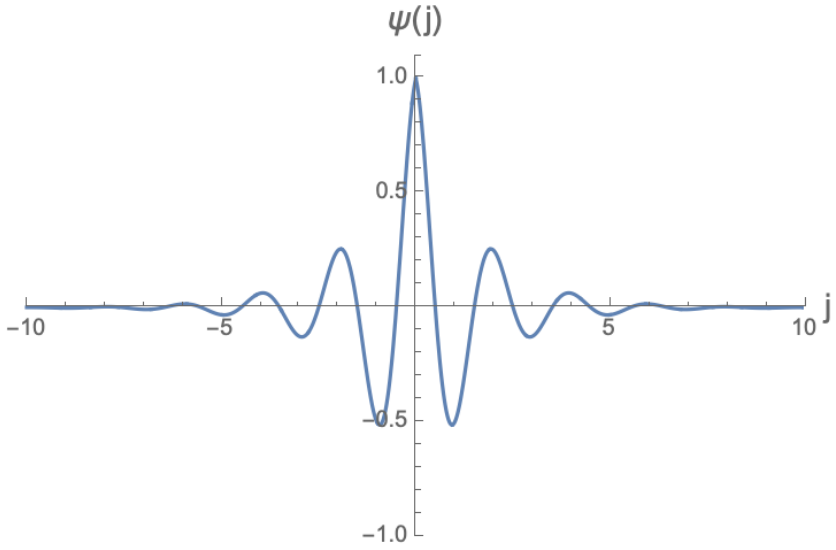

$$\psi_L = e^{-ik_0 j} = e^{-i(i\ln\tau)j} = e^{\ln\tau j}. \tag{5.69}$$

We can confirm that there is indeed one bound state by checking with the Levinson's theorem once again. The phase of the transmission amplitude t_k, τ_k is

$$\tau_k = \arctan\frac{1-\tau^2}{2\tau\sin k}, \tag{5.70}$$

which in the $\lim_{k\to 0}$, $\tau(0) = \pi/2$. Using the Levinson's theorem we once again find the number of bound states, $n_b = 1$.

5.5 Chapter summary

We first defined the explicit nature of the bound state using scattering amplitudes. We observed that the single bound state found is localised around the potential with the wavefunctions exponentially decaying away from the centre of the chain (placement of potential). The total charge is also calculated and is found to be 0 for $\lambda < 0$ in the case that a bound

Figure 5.4: The wavefunction for $\tau > 1$ is the bound state that we are looking for. It is shown to be localised about the centre and then exponentially decaying far from the origin.

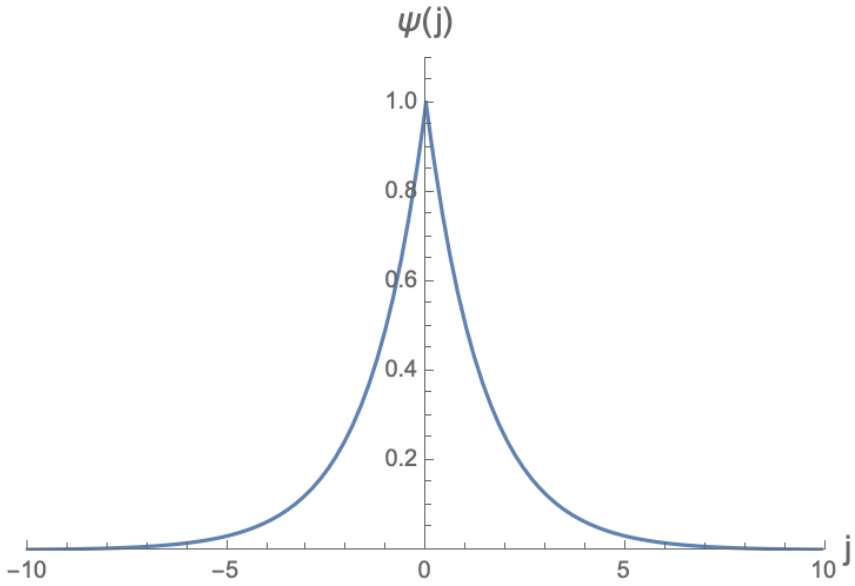

state is present, and -1 otherwise. We also confirmed that there is only one bound state present for a Bravais lattice by repeating the steps for the continuous chain. Finally we were able to find the bound state for the SSH model which is present for $\tau > 1$.

Chapter 6

Density of states via the S-Matrix

In this section we obtain the number of bound states though the density of states of the system. We define the density of states as the total states available in the system for a given eigen-energy, ε. To obtain the bound states, we begin with defining the Scattering Matrix (or S-Matrix) [57] which is a 2x2 matrix that describes the outgoing waves of a one-dimensional system with a centred potential, in terms of the incoming waves. We can also write the amplitudes of the waves to the left side of the potential in terms of those on the right side, which defines the T-matrix. It can be thought of as the effective potential which is the potential that is modified due to multiple scattering. Since we work in a one-dimensional system, the wave in both the left and right sides of the potential has two components, one moving to the right and one moving to the left, therefore the T-matrix is also a 2x2 matrix.

The phase of these amplitudes, in particular, the transmission amplitude, can give information about the number of bound states in our system. This is in combination with the sum rule, or alternatively as we have also seen, with the one-dimensional Levinson's theorem. We also define properties of the S-matrix such as unitarity and time reversal symmetry (TRS) which contributes significantly to quantifying bound states.

6.1 General reduction to T-Matrix

To begin with we define the density of states (or DoS) which describes the number of states available in a system for a given eigen-energy ε:

$$\nu(\varepsilon) = \sum_n \delta(\varepsilon - \varepsilon_n) = \mathrm{Tr}\,\delta(\varepsilon - H), \tag{6.1}$$

with Hamiltonian $H = H_0 + V$, where H_0 is the Hamiltonian of the unperturbed system. The Green's functions which represent the response to the δ-function,

$$G^R = \frac{1}{\varepsilon + i0 - H},\ G^A = \frac{1}{\varepsilon - i0 - H},\ G_0^R = \frac{1}{\varepsilon + i0 - H_0},\ G_0^R = \frac{1}{\varepsilon - i0 - H_0}, \tag{6.2}$$

where G^R and G^A are retarded and advanced Green's functions respectively, can be used to re-write the DoS:

$$\nu(\varepsilon) = -\frac{1}{2\pi i}\,\mathrm{Tr}\big(G^R - G^A\big). \tag{6.3}$$

The following is true for either retarded or advances Green's functions:

$$\begin{aligned} G^{-1} &= G_0^{-1} - V = [1 - VG_0]G_0^{-1} \\ G &= G_0[1 - VG_0]^{-1} = G_0 + G_0VG \end{aligned} \tag{6.4}$$

and

$$G = G_0 \sum_{n=0}^{\infty}(VG_0)^n = G_0 + G_0TG_0,\ T = V\sum_{n=0}^{\infty}(G_0V)^n = V[1 - G_0V] - 1. \tag{6.5}$$

The excess DoS, $\delta\nu = \nu - \nu_0$, can be written as:

$$\delta\nu = -\frac{1}{2\pi i}\,\mathrm{Tr}\big(G_0^RT^RG_0^R - G_0^AT^AG_0^A\big). \tag{6.6}$$

We can first deal with the retarded contribution:

$$\mathrm{Tr}\big(G_0^RT^RG_0^R\big) = -\,\mathrm{Tr}\,\frac{dG_0^R}{d\varepsilon}T^R = -\,\mathrm{Tr}\,\frac{dG_0^R}{d\varepsilon}V\sum_{n=0}^{\infty}(G_0^RV)^n \tag{6.7}$$

$$= -\frac{d}{d\varepsilon}\,\mathrm{Tr}\sum_{n=0}^{\infty}\frac{1}{n}(G_0^R V)^n = \frac{d}{d\varepsilon}\,\mathrm{Tr}\ln\left[1 - G_0^R V\right]. \tag{6.8}$$

This leads to,

$$\delta\nu = -\frac{1}{2\pi i}\frac{d}{d\varepsilon}\,\mathrm{Tr}\ln\left(1 - G_0^A V)(1 - G_0^R V\right)^{-1}. \tag{6.9}$$

We can manipulate the inverse as an infinite series like so:

$$(1 - G_0^A V)(1 - G_0^R V)^{-1} = 1 + \Delta G_0 T, \tag{6.10}$$

where $T = T^R$ but this subscript is not important since T-matrix is not singular such that both T and T^R can be multiplied by their inverses to give the identity matrix, and

$$\Delta G_0 = G_0^R - G_0^A = -2\pi i\delta(\varepsilon - H_0). \tag{6.11}$$

We can immediately obtain,

$$\delta\nu = -\frac{1}{2\pi i}\frac{d}{d\varepsilon}\,\mathrm{Tr}\ln\left[1 - 2\pi i\delta(\varepsilon - H_0)T\right]. \tag{6.12}$$

Expanding log and taking Tr in the basis of plane waves with wave-vector k_i,

$$\mathrm{Tr}[\delta(\varepsilon - H_0)T]^n = \int d^n k\,\langle k_1|\,\delta(\varepsilon - H_0)T\,|k_2\rangle\,...\,\langle n_1|\,\delta(\varepsilon - H_0)T\,|k_1\rangle \tag{6.13}$$

$$= \int d^n l\delta(\varepsilon - \varepsilon_{k_1})\,\langle k_1|\,T\,|k_2\rangle\,...\delta(\varepsilon - \varepsilon_{k_{n_1}})\,\langle k_{n-1}|\,T\,|k_1\rangle \tag{6.14}$$

$$= (\nu_0(\varepsilon)/2)^n \sum_{\sigma}\langle\sigma_1 k|\,T\,|\sigma_2 k\rangle\,...\,\langle\sigma_{n-1}k|\,T\,|\sigma_1 k\rangle = (\nu_0(\varepsilon)/2)^n\,\mathrm{tr}\,t^n, \tag{6.15}$$

where $\sigma = \pm 1$, vector $k = k(\varepsilon)$ is the solution of he equation $\varepsilon(k) = \varepsilon$ which we assume to have two solutions, σk, and Tr is the trace summing over all energies. We also define,

$$\nu_0(\varepsilon) = 1/\pi|v(\varepsilon)| = (1/\pi)dk(\varepsilon)/d\varepsilon \tag{6.16}$$

with $v(\varepsilon)$ being velocity at energy ε.

As we can see, the T-matrix is needed on-shell only, i.e. we only need to find its matrix elements between two states with fixed energy ε. Little trace is taken over this small space since we now have fixed energy:

$$\delta\nu = \frac{1}{2\pi i}\frac{d}{d\varepsilon}\operatorname{tr}\ln\left[1 - i\pi\nu_0(\varepsilon)t\right], \quad t_{\sigma\sigma'} = \left\langle \sigma k(\varepsilon)\right| T \left|\sigma' k(\varepsilon)\right\rangle . \tag{6.17}$$

6.1.1 Meaning of T-Matrix

Any eigenstate of the Hamiltonian H is built from the unperturbed state (eigenstates of the Hamiltonian H_0) as:

$$|\psi\rangle = \left[1 + G_0^R T^R\right]|\psi_0\rangle . \tag{6.18}$$

Taking plane wave with momentum $k \equiv k(\varepsilon)$ as an eigenstate of H_0, we can build a scattering state:

$$|\psi\rangle = \left[1 + G_0^R T^R\right]|k\rangle , \ \langle x|k\rangle = e^{ikx}. \tag{6.19}$$

In x-representation we have:

$$\langle x|\psi\rangle = e^{ikx} + \int dx' G_0^R(x - x')\left\langle x'\right| T^R \left|k\right\rangle . \tag{6.20}$$

We can find asymptotic behaviour of solutions at $x \to \pm\infty$. Since only poles can give a finite result to the spectrum ε_p can be linearised around the points $\varepsilon = \varepsilon_p$ making the contributions to the integral:

$$G_0^R(x - x') = \int \frac{dp}{2\pi}\frac{e^{ip(x-x')}}{\varepsilon + i0 - \varepsilon_p} = \frac{\pi\nu_0(\varepsilon)}{2\pi}\int d\varepsilon \frac{e^{i\varepsilon(x-x')}}{\varepsilon + i0 - \varepsilon_p} \tag{6.21}$$

$$= \frac{2\pi i\nu_0(\varepsilon)}{2} e^{i\varepsilon_p(x-x')} = -i\pi\nu_0(\varepsilon)e^{ik(\varepsilon)|x-x'|}, \tag{6.22}$$

in the limit $x \to \pm\infty$. Here $k(\varepsilon)$ is the solution of $\varepsilon = \varepsilon_k$ corresponding to the right-moving wave, i.e. the point with

$$v(\varepsilon) = \frac{d\varepsilon}{dk}\Big|_{\varepsilon=\varepsilon_k} > 0. \tag{6.23}$$

For the waves incoming from the left for $x \to +\infty$:

$$\langle x|\psi\rangle = e^{ikx} - i\pi\nu_0 e^{ikx} \int dx' e^{-ikx'} \left\langle x'\right| T^R \left|k\right\rangle = e^{ikx} - i\pi\nu_0 e^{ikx} \left\langle k\right| T^R \left|k\right\rangle, \tag{6.24}$$

and for $x \to -\infty$:

$$\langle x|\psi\rangle = e^{ikx} - i\pi\nu_0 e^{-ikx} \int dx' e^{ikx'} \left\langle x'\right| T^R \left|k\right\rangle = e^{ikx} - i\pi\nu_0 e^{-ikx} \left\langle -k\right| T^R \left|k\right\rangle. \tag{6.25}$$

Therefore, scattering amplitudes for right-moving (incoming from the left) waves are:

$$\begin{aligned} t &= 1 - i\pi\nu_0 \left\langle k\right| T^R \left|k\right\rangle, \\ r &= -i\pi\nu_0 \left\langle -k\right| T^R \left|k\right\rangle. \end{aligned} \tag{6.26}$$

Repeating similar calculation for left-moving (incoming from the right), we can find similar scattering amplitudes:

$$\begin{aligned} t' &= 1 - i\pi\nu_0 \left\langle -k\right| T^R \left|-k\right\rangle, \\ r' &= -i\pi\nu_0 \left\langle k\right| T^R \left|-k\right\rangle. \end{aligned} \tag{6.27}$$

We can define on-shell S-matrix:

$$S_{\sigma\sigma'} = \delta_{\sigma\sigma'} - i\pi\nu_0 \left\langle \sigma k\right| T^R \left|\sigma' k\right\rangle, \tag{6.28}$$

$$S = \begin{pmatrix} t & r' \\ r & t' \end{pmatrix}, \tag{6.29}$$

and the required result becomes:

$$\delta\nu(\varepsilon) = \frac{1}{2\pi i}\frac{d}{d\varepsilon} tr \ln S. \tag{6.30}$$

6.1.2 S-matrix properties

The S-matrix is unitary due to the fact that probabilities are conserved across the scattering process,

$$S^{\dagger}S = 1. \tag{6.31}$$

Time reversal symmetry (TRS) i.e. the complex conjugate of an eigenfunction is also an eigenfunction, means:

$$S^{T} = \sigma_1 S \sigma_1. \tag{6.32}$$

For a TRS situation:

$$\delta\nu(\varepsilon) = \frac{1}{\pi}\frac{d\theta}{d\varepsilon}, \tag{6.33}$$

where θ is the phase of the transmission amplitude.

6.2 Chapter summary

We derived the excess density of states in terms of the transfer matrix. This allowed us to then define the s-matrix, or scattering matrix, and write the excess density of states in terms of it. The s-matrix is useful since it contains the reflection and transmission amplitudes which can describe the nature of the topology of the system.

Chapter 7

Density of states via the continuity equation

In this section, we will present an alternative approach to Levinson's theorem in order to determine the bound states of a system. We will do this by exploiting the continuity equation [59] and expressing the total number of states

$$\int_{-\infty}^{+\infty} dx|\psi_\varepsilon(x)|^2 \tag{7.1}$$

in terms of asymptotic behaviour, i.e. in terms of reflection and transmission amplitudes.

In operator form the continuity equation is written as:

$$\partial_t \hat{n}(x,t) + \partial_x \hat{j}(x,t) = 0, \tag{7.2}$$

where

$$\hat{n}(x,t) = e^{i\hat{H}t}\hat{n}(x)e^{-i\hat{H}t}, \quad \hat{n}(x) = \delta(x-\hat{x}), \tag{7.3}$$

$$\hat{j}(x,t) = e^{i\hat{H}t}\hat{j}(x)e^{-i\hat{H}t}, \quad \hat{j}(x) = \frac{1}{2}[\hat{v}\delta(x-\hat{x}) + \delta(x-\hat{x})\hat{v}]. \tag{7.4}$$

Taking matrix elements,

$$\langle\varepsilon|\,\hat{n}(x,t)\,|\varepsilon'\rangle = e^{-i(\varepsilon'-\varepsilon)t}\bar{\psi}_{\varepsilon}(x)\psi_{\varepsilon'}(x), \tag{7.5}$$

$$\langle\varepsilon|\,\hat{j}(x,t)\,|\varepsilon'\rangle = e^{-i(\varepsilon'-\varepsilon)t}j_{\varepsilon\varepsilon'}(x), \tag{7.6}$$

$$j_{\varepsilon\varepsilon'}(x) = \frac{-i}{2}[\bar{\psi}_{\varepsilon}(x)\partial_x\psi_{\varepsilon'}(x) - \partial_x\bar{\psi}_{\varepsilon}(x)\psi_{\varepsilon'}(x)], \tag{7.7}$$

where we assume unit particle mass. The continuity equation for matrix elements can be found as:

$$\partial_t\,\langle\varepsilon|\,\hat{n}(x,t)\,|\varepsilon'\rangle + \partial_x\,\langle\varepsilon|\,\hat{j}(x,t)\,|\varepsilon'\rangle = 0. \tag{7.8}$$

Therefore, it is solved to be:

$$\bar{\psi}_{\varepsilon}(x)\psi_{\varepsilon'}(x) = -\frac{i}{\varepsilon'-\varepsilon}\partial_x j_{\varepsilon\varepsilon'}(x), \tag{7.9}$$

and can be integrated between two distance points $\pm L/2$ that are outside of the scattering region,

$$\int_{-L/2}^{L/2} dx\bar{\psi}_{\varepsilon}(x)\psi_{\varepsilon'}(x) = -\frac{i}{\varepsilon'-\varepsilon}[j_{\varepsilon\varepsilon'}(L/2) - j_{\varepsilon\varepsilon'}(-L/2)]. \tag{7.10}$$

The waves incoming from the left are:

$$j_{\varepsilon\varepsilon'}(x\to+\infty) = k_+\bar{t}_{\varepsilon}t_{\varepsilon'}e^{2ik_-x}, \tag{7.11}$$

$$j_{\varepsilon\varepsilon'}(x\to-\infty) = k_+[e^{2ik_-x} - \bar{r}_{\varepsilon}r_{\varepsilon'}e^{-2ik_-x}] + k_-[\bar{r}_{\varepsilon}e^{2ik_+x} - r_{\varepsilon'}e^{-2ik_+x}]; \tag{7.12}$$

which we obtain by substituting $\psi_R = t_k e^{ikx}$ and $\psi_L = e^{ikx} + r_k e^{-ikx}$ into Eq. (7.7). Similarly, from the right:

$$j'_{\varepsilon\varepsilon'}(x\to-\infty) = -k_+\bar{t}_{\varepsilon}t_{\varepsilon'}e^{-2ik_-x}, \tag{7.13}$$

$$j'_{\varepsilon\varepsilon'}(x\to+\infty) = -k_+[e^{-2ik_-x} - \bar{r}_{\varepsilon}r_{\varepsilon'}e^{2ik_-x}] - k_-[\bar{r}_{\varepsilon}e^{-2ik_+x} - r_{\varepsilon'}e^{2ik_+x}]; \tag{7.14}$$

where

$$k_{\pm} = \frac{1}{2}[k(\varepsilon') \pm k(\varepsilon)]. \tag{7.15}$$

To take the limit $\varepsilon' - \varepsilon = \omega \to 0$, we take Eq. (7.10) and substitute Eq's. (7.11), (7.12) to find:

$$\int_{-L/2}^{L/2} dx \bar{\psi}_{\varepsilon}(x)\psi_{\varepsilon'}(x) = -\frac{i}{\varepsilon' - \varepsilon}\Big[k_+ \bar{t}_{\varepsilon} t_{\varepsilon'} e^{ik_- L} - k_+[e^{-ik_- L} - \bar{r}_{\varepsilon} r_{\varepsilon'} e^{ik_- L}] - k_-[\bar{r}_{\varepsilon} e^{-ik_+ L} - r_{\varepsilon'} e^{ik_+ L}]\Big]. \tag{7.16}$$

Using $\varepsilon = k(\varepsilon)^2/2$ gives

$$\frac{i}{\varepsilon' - \varepsilon} = \frac{i}{\frac{1}{2}(k^2(\varepsilon') - k^2(\varepsilon))} = \frac{i}{2k_+ k_-}. \tag{7.17}$$

Therefore, we get

$$\int_{-L/2}^{L/2} dx \bar{\psi}_{\varepsilon}(x)\psi_{\varepsilon'}(x) = -\frac{i}{2}\Big[\frac{\bar{t}_{\varepsilon} t_{\varepsilon'}}{k_-} e^{ik_- L} - \frac{1}{k_-}[e^{-ik_- L} - \bar{r}_{\varepsilon} r_{\varepsilon'} e^{ik_- L}] - \frac{1}{k_+}[\bar{r}_{\varepsilon} e^{-ik_+ L} - r_{\varepsilon'} e^{ik_+ L}]\Big]. \tag{7.18}$$

Now to take the limits. Since we are taking the limit $\varepsilon' - \varepsilon \to 0$, the result for k_+ becomes

$$k_+ = \frac{1}{2}(k(\varepsilon') + k(\varepsilon)) \approx k(\varepsilon). \tag{7.19}$$

For k_-, we take into account the exponential, and expand for small k_- which gives

$$\lim_{\varepsilon' \to \varepsilon} \frac{e^{ik_- L}}{k_-} \approx \frac{1}{k_-} + iL, \tag{7.20}$$

and

$$\lim_{\varepsilon' \to \varepsilon} \frac{e^{-ik_- L}}{k_-} \approx \frac{1}{k_-} - iL. \tag{7.21}$$

Using the results, we get

$$\int_{-L/2}^{L/2} dx\bar{\psi}_\varepsilon(x)\psi_{\varepsilon'}(x) = -\frac{i}{2}\Big[\bar{t}_\varepsilon\Big(\frac{1}{k_-}+iL\Big)t_{\varepsilon'} - \frac{1}{k_-}+iL \\ + \bar{r}_\varepsilon\Big(\frac{1}{k_-}+iL\Big)r_{\varepsilon'} - \frac{1}{k}\Big(\bar{r}e^{-ikL} - re^{ikL}\Big)\Big] \quad (7.22)$$

$$= -\frac{i}{2}\Big[\bar{t}_\varepsilon\Big(\frac{1}{k_-}+iL\Big)t_{\varepsilon'} - \frac{1}{k_-}+iL + \bar{r}_\varepsilon\Big(\frac{1}{k_-}+iL\Big)r_{\varepsilon'}\Big] + \frac{1}{2ik}\Big(re^{ikL} - \bar{r}e^{-ikL}\Big). \quad (7.23)$$

Looking only at the iL terms, the result is

$$-\frac{i}{2}\Big[\bar{t}iLt + iL + \bar{r}iLr\Big] = \frac{L}{2}\Big[\bar{t}t + 1 + \bar{r}r\Big] = L, \quad (7.24)$$

since $\bar{t}t + \bar{r}r = |t|^2 + |r|^2 = 1$. Now looking at the $1/k_-$ terms and writing $\varepsilon' = \varepsilon + \omega$ gives

$$-\frac{i}{2k_-}\Big[\bar{t}_\varepsilon t_{\varepsilon+\omega} + \bar{r}_\varepsilon r_{\varepsilon+\omega} - 1\Big] = -\frac{i}{2}\left[\frac{2\Big(\bar{t}_\varepsilon t_{\varepsilon+\omega} + \bar{r}_\varepsilon r_{\varepsilon+\omega} - 1\Big)}{k_{\varepsilon+\omega} - k_\varepsilon}\right]. \quad (7.25)$$

Since this vanishes as $\omega \to 0$, L'Hopital's rule must be applied to give

$$-i\lim_{\omega\to 0}\left[\frac{\Big(\bar{t}_\varepsilon t_{\varepsilon+\omega} + \bar{r}_\varepsilon r_{\varepsilon+\omega} - 1\Big)}{k_{\varepsilon+\omega} - k_\varepsilon}\right] = -i\left[\frac{\partial_\omega\Big(\bar{t}_\varepsilon t_{\varepsilon+\omega} + \bar{r}_\varepsilon r_{\varepsilon+\omega} - 1\Big)}{\partial_\omega\Big(k_{\varepsilon+\omega} - k_\varepsilon\Big)}\right] \quad (7.26)$$

$$= -i\left[\frac{\bar{t}_\varepsilon\partial_\omega t_{\varepsilon+\omega} + \bar{r}_\varepsilon\partial_\omega r_{\varepsilon+\omega}}{\partial_\omega k_{\varepsilon+\omega}}\right]. \quad (7.27)$$

Now since $\omega \to 0$, an expansion about ε can be taken such that

$$\partial_\omega t_{\varepsilon+\omega} \approx \partial_\omega\Big(t(\varepsilon) + \omega\partial_\varepsilon t(\varepsilon)\Big) = \partial_\varepsilon t(\varepsilon). \quad (7.28)$$

This can be substituted in to give

$$-i\left[\frac{\bar{t}_\varepsilon\partial_\omega t_{\varepsilon+\omega} + \bar{r}_\varepsilon\partial_\omega r_{\varepsilon+\omega}}{\partial_\omega k_{\varepsilon+\omega}}\right] = -i\left[\frac{\bar{t}_\varepsilon\partial_\varepsilon t_\varepsilon + \bar{r}_\varepsilon\partial_\varepsilon r_\varepsilon}{\partial_\varepsilon k_\varepsilon}\right], \quad (7.29)$$

therefore since

$$\frac{d\varepsilon}{dk}\frac{d}{d\varepsilon} = \frac{d}{dk} = \partial_k, \tag{7.30}$$

we get

$$-i\left[\frac{\bar{t}_\varepsilon \partial_\varepsilon t_\varepsilon + \bar{r}_\varepsilon \partial_\varepsilon r_\varepsilon}{\partial_\varepsilon k_\varepsilon}\right] = -i\Big(\bar{t}_\varepsilon \partial_k t_\varepsilon + \bar{r}_\varepsilon \partial_k r_\varepsilon\Big). \tag{7.31}$$

Combining this together we get

$$\int_{-L/2}^{L/2} dx \bar{\psi}_\varepsilon(x)\psi_{\varepsilon'}(x) \to \int_{-L/2}^{L/2} dx |\psi_\varepsilon(x)|^2 \tag{7.32}$$

$$= L - i\Big(\bar{t}_\varepsilon \partial_k t_\varepsilon + \bar{r}_\varepsilon \partial_k r_\varepsilon\Big) + \frac{1}{2ik}\Big(re^{ikL} - \bar{r}e^{-ikL}\Big) \tag{7.33}$$

for waves incoming from the left.

For the waves incoming from the right, we have

$$\int_{-L/2}^{L/2} dx \bar{\psi}_\varepsilon(x)\psi_{\varepsilon'}(x) = -\frac{i}{2k_+k_-}\Big[- k_+[e^{-ik_-L} - \bar{r}_\varepsilon r_{\varepsilon'} e^{ik_-L}] - k_-[\bar{r}_\varepsilon e^{-ik_+L} - r_{\varepsilon'} e^{ik_+L}] - \Big(- k_+ \bar{t}_\varepsilon t_{\varepsilon'} e^{ik_-L}\Big)\Big], \tag{7.34}$$

using Eq's. (7.13) and (7.14).

By performing the same expansion as above, we get

$$\int_{-L/2}^{L/2} dx \bar{\psi}_\varepsilon(x)\psi_{\varepsilon'}(x) = -\frac{i}{2}\Big[- \frac{1}{k_-} + iL + \bar{r}_\varepsilon r_{\varepsilon'}\Big(\frac{1}{k_-} + iL\Big) - \frac{1}{k_+}[\bar{r}_\varepsilon e^{-ik_+L} - r_{\varepsilon'} e^{ik_+L}] + \bar{t}_\varepsilon t_{\varepsilon'}\Big(\frac{1}{k_-} + iL\Big)\Big]. \tag{7.35}$$

As before, the $1/k_+$ terms as $\varepsilon' \to \varepsilon$ become

$$-\frac{i}{2}\Big[\frac{1}{k_+}[r_{\varepsilon'} e^{ik_+L} - \bar{r}_\varepsilon e^{-ik_+L}]\Big] = \frac{1}{2ik}[re^{ikL} - \bar{r}e^{-ikL}]. \tag{7.36}$$

Similarly, the iL terms become

$$-\frac{i}{2}\Big[iL(1+\bar{r}_\varepsilon r_{\varepsilon'}+\bar{t}_\varepsilon t_{\varepsilon'})\Big]=L. \tag{7.37}$$

For the $1/k_-$ terms, they are the same as above, so L'Hopitals rule can be applied and the same manipulations can be used by taking the limit $\varepsilon'\to\varepsilon$ to give

$$-\frac{i}{2}\Big[\frac{1}{k_-}(-1+\bar{r}_\varepsilon r_{\varepsilon'}+\bar{t}_\varepsilon t_{\varepsilon'}\Big]=-i\Big(\bar{t}\partial_k t+\bar{r}\partial_k r\Big). \tag{7.38}$$

Since these waves move in a different direction, primes must be included for the reflection and transmission coefficient, and wave-functions. Subsequently, the final result is

$$\int_{-L/2}^{L/2}dx\bar{\psi}'_\varepsilon(x)\psi'_{\varepsilon'}(x)\to\int_{-L/2}^{L/2}dx\big|\psi'_\varepsilon(x)\big|^2=L-\Big(\bar{t}'\partial_k t'+\bar{r}'\partial r'\Big)+\frac{1}{2ik}(r'e^{ikL}-\bar{r}'e^{-ikL}). \tag{7.39}$$

Finally, we re-state our results for clarity:

$$\int_{-L/2}^{L/2}dx|\psi_\varepsilon(x)|^2=L-i\Big(\bar{t}_\varepsilon\partial_k t_\varepsilon+\bar{r}_\varepsilon\partial_k r_\varepsilon\Big)+\frac{1}{2ik}\Big(re^{ikL}-\bar{r}e^{-ikL}\Big) \tag{7.40}$$

$$\int_{-L/2}^{L/2}dx\big|\psi'_\varepsilon(x)\big|^2=L-\Big(\bar{t}'\partial_k t'+\bar{r}'\partial r'\Big)+\frac{1}{2ik}(r'e^{ikL}-\bar{r}'e^{-ikL}). \tag{7.41}$$

Since we are going to integrate over k later and L is a large parameter, contributions from $k\geq L^{-1}$ will be suppressed, and for a function of k we have:

$$\frac{1}{k}e^{ikL}\to i\pi\delta(k). \tag{7.42}$$

This gives us the final result:

$$\int_{-L/2}^{L/2}[|\psi_\varepsilon(x)|^2+\left|\psi'_\varepsilon(x)\right|^2]dx-2L \tag{7.43}$$

$$=-i(\bar{r}\partial_k r+\bar{t}\partial_k t+\bar{r}'\partial_k r'+\bar{t}'\partial_k t')+\frac{\pi}{2}(r_0+\bar{r}_0+r'_0+\bar{r}'_0)\delta(k). \tag{7.44}$$

Here index 0 represents $\varepsilon=0$ or $(k=0)$. Since $\psi^{(0)}_\varepsilon(x)=e^{ikx}$ and $\psi'_\varepsilon(x)=e^{-ikx}$, the LHS

$$\int_{-L/2}^{L/2}[|\psi_\varepsilon(x)|^2+\left|\psi'_\varepsilon(x)\right|^2]dx-2L=\int_{-L/2}^{L/2}[\left|\psi^{(0)}_\varepsilon(x)\right|^2+\left|\psi'^{(0)}_\varepsilon(x)\right|^2]dx-2L, \tag{7.45}$$

has the finite limit when $L=\infty$. This limit, δn_k, can be written as:

$$\delta n_k=-i(\bar{r}\partial_k r+\bar{t}\partial_k t+\bar{r}'\partial_k r'+\bar{t}'\partial_k t')+\frac{\pi}{2}(r_0+\bar{r}_0+r'_0+\bar{r}'_0)\delta(k) \tag{7.46}$$

where

$$\bar{r}\partial_k r+\bar{t}\partial_k t+\bar{r}'\partial_k r'+\bar{t}'\partial_k t'=\operatorname{tr}\hat{S}^\dagger_k\partial_k\hat{S}_k=\partial_k\ln\det\hat{S}_k. \tag{7.47}$$

Notation $\det\hat{S}_k=e^{2i\delta_k}$ reduces the formula above to:

$$\delta n_k=-i\partial_k\ln e^{2i\delta_k}++\frac{\pi}{2}(r_0+\bar{r}_0+r'_0+\bar{r}'_0)\delta(k) \tag{7.48}$$

$$=2\partial_k\delta_k+\frac{\pi}{2}(r_0+\bar{r}_0+r'_0+\bar{r}'_0)\delta(k). \tag{7.49}$$

We also use the relation $r(k)=\bar{r}(-k)$ which means that $r_0\equiv r(k=0)$ is real:

$$\delta n_k=2\partial_k\delta_k+\pi(r_0+r'_0)\delta(k). \tag{7.50}$$

The sum rule, which can give us the total number of bound states;

$$\int_\infty^\infty dx\Big[\sum_{n=1}^{n_b}|\psi_n(x)|^2+\int_0^\infty\frac{dk}{2\pi}(|\psi_\varepsilon(x)|^2+\left|\psi'_\varepsilon(x)\right|^2)\Big] \tag{7.51}$$

$$=n_b+\int_\infty^\infty dx\int_0^\infty\frac{dk}{2\pi}\Big(\left|\psi^{(0)}_\varepsilon(x)\right|^2+\left|\psi'^{(0)}_\varepsilon(x)\right|^2\Big), \tag{7.52}$$

becomes

$$n_b = \frac{1}{2\pi}[\delta_{k=0} - \delta_{k=\infty}] - \frac{1}{4}(r_0 + r_0'). \tag{7.53}$$

If there is time reversal symmetry, the phase of the determinant is equal to the phase of the transmission amplitude:

$$\delta_{k=0} = \theta_t(k),\ t(k) = \sqrt{T_k}e^{i\theta(k)}, \tag{7.54}$$

and the number of bound states:

$$n_b = \frac{1}{\pi}[\theta_t(k=0) - \theta_t(k=\infty)] - \frac{1}{4}(r_0 + r_0'). \tag{7.55}$$

7.1 Application to the continuous Schrödinger equation with δ-function potential

The scattering amplitudes amplitudes derived in section 6.1 are

$$r_k = \frac{-\lambda}{\lambda + 2ik}, \quad t_k = \frac{2k}{2k - i\lambda}. \tag{7.56}$$

We can define:

$$\theta_t(k=0) = \frac{\pi}{2}\,\mathrm{sign}\,\lambda, \quad \theta_t(k=\infty) = 0 \tag{7.57}$$

$$r(k=0) = r'(k=0) = -1 \tag{7.58}$$

where Eq. (7.58) holds due to time reversal symmetry, then this leads to:

$$n_b = \frac{1}{2}[\mathrm{sign}\,\lambda + 1] \tag{7.59}$$

7.2 Chapter summary

The continuity equation is exploited to give useful insight on the possible bound states of a system. In the asymptotic limit, the sum rule was reduced to a simple expression giving the number of bound states in terms of the reflection amplitude and the phase of the transmission amplitude. This was applied to the one-dimensional continuous Schrödinger equation with a δ-function potential, and it was found that the number of bound states is 1 if the amplitude $\lambda = +1$.

Chapter 8

Bound states for Bravais lattice with arbitrary hopping

In this section we aim to derive the number of bound states for arbitrary, or long-range hopping in which particles may jump beyond nearest-neighbour sites. This is done for the Bravais (or, simple) lattice in which all lattice sites are identical. The Hamiltonian is given as,

$$\hat{H} = \hat{H}_0 + \hat{V}, \tag{8.1}$$

where

$$\hat{H}_0 = \sum_{x,x'} t_{x-x'} \left|x\right\rangle \left\langle x'\right|, \quad t_{x-x'} = t_{x'-x} = \bar{t}_{x-x'}, \tag{8.2}$$

$$\hat{V} = \sum_{x} \left|x\right\rangle \left\langle x\right|. \tag{8.3}$$

We set the condition that the perturbation exists near the edge, i.e. $V_{x\to\infty} = 0$. The current operator on a link is found from

$$\hat{j}_{x+1/2} = -\partial_t \hat{N}_x, \quad \hat{N}_x = \sum_{l\leq x} \left|l\right\rangle \left\langle l\right|. \tag{8.4}$$

$$\hat{j}_{x+1/2} = -i[\hat{H}, N_x] = -i[\hat{H}_0, N_x] = i \sum_{l\leq x<r} t_{r-l}\Big[\left|l\right\rangle \left\langle r\right| - \left\langle r|l\right\rangle \Big] \tag{8.5}$$

with matrix element

$$\langle\varepsilon|\,\hat{j}_{x+1/2}\,\big|\varepsilon'\big\rangle = i\sum_{l\le x<r} t_{r-l}[\langle\varepsilon|l\rangle\,\big\langle r\big|\varepsilon'\big\rangle - \langle\varepsilon|r\rangle\,\big\langle l\big|\varepsilon'\big\rangle]. \tag{8.6}$$

The continuity equation

$$i\omega\,\langle\varepsilon|\,\hat{N}_x\,|\varepsilon+\omega\rangle = \langle\varepsilon|\,\hat{j}_{x+1/2}\,|\varepsilon+\omega\rangle \tag{8.7}$$

in the limit $\omega \to 0$ becomes

$$\langle\varepsilon|\,\hat{j}_{x+1/2}\,|\varepsilon\rangle = 0 \tag{8.8}$$

and

$$\langle\varepsilon|\,\hat{N}\,\big|\varepsilon'\big\rangle = -i\,\langle\varepsilon|\,\hat{j}_{x+1/2}\partial_\varepsilon\,|\varepsilon\rangle\,, \tag{8.9}$$

where

$$\langle\varepsilon|\,\hat{j}_{x+1/2}\partial_\varepsilon\,|\varepsilon\rangle = i\sum_{l\le x<r} t_{r-l}\Big[\,\langle\varepsilon|l\rangle\,\partial_\varepsilon\,\langle r|\varepsilon\rangle - \langle\varepsilon|r\rangle\,\partial_\varepsilon\,\langle l|\varepsilon\rangle\,\Big] \tag{8.10}$$

and Eq. (8.9) has been adapted from Eq.'s (7.40) and (7.41).

8.1 Total number of states

For a simple lattice with one site per unit cell,

$$\langle x|\varepsilon\rangle = \sum_i a_i e^{ik_i x}, \tag{8.11}$$

where $k_i = k_i(\varepsilon)$ is a root of $\varepsilon_k = \varepsilon$,

$$a_i = a_{k=k_i(\varepsilon)}, \quad \varepsilon_k = 2\sum_{d=1}^{\infty} t_d \cos kd. \tag{8.12}$$

Using Eq. (8.8), we find that $J_{i,j} = \delta_{ij} v_i$. To prove this we define

$$j_\varepsilon \equiv \langle \varepsilon | \, \hat{j}_\xi \, | \varepsilon \rangle = \sum_{i,j} J_{i,j} \bar{a}_i a_j, \quad \xi \equiv x + 1/2 \tag{8.13}$$

where

$$J_{i,j} = i \sum_{l \le x < r} t_{r-l} \Big[e^{ik_i l + ik_j r} - e^{ik_i r + ik_j l} \Big]. \tag{8.14}$$

Using notation

$$\sum_{l \le x < r} = \sum_{d=1}^{\infty} \sum_{y=-(d-1)}^{d-1}, \tag{8.15}$$

where $r - l = d$, $r + l = 2x + 1 + y$.

$$J_{i,j} = -2e^{-ik_{ij}(x+1/2)} \sum_{d=1}^{\infty} t_d \sin \frac{k_i + k_j}{2} d \sum_{y=-(d-1)}^{d-1} e^{-ik_{ij} y/2} \tag{8.16}$$

$$= -\frac{2e^{-ik_{ij}(x+1/2)}}{\sin k_{ij}/2} \sum_{d=1}^{\infty} t_d \sin \frac{k_i + k_j}{2} d \sin \frac{k_{ij}}{2} d, \tag{8.17}$$

where $k_{ij} = k_i - k_j$.

If $i \neq j$,

$$\begin{aligned} \sum_{d=1}^{\infty} t_d \sin \frac{k_i + k_j}{2} d \sin \frac{k_i - k_j}{2} d = \frac{1}{2} \sum_{d=1}^{\infty} t_d [\cos k_j d - \cos k_i d] = \frac{1}{4} [\varepsilon(k_j) - \varepsilon(k_i)] \\ = \frac{\varepsilon - \varepsilon}{4} = 0 \end{aligned} \tag{8.18}$$

If $i = j$, then using L'Hopital's rule

$$\frac{\sin k_{ij} d/2}{\sin k_{ij}/2} \to d \tag{8.19}$$

$$J_{i,j} = -2 \sum_{d=1}^{\infty} t_d d \sin k_i d = \frac{\partial \varepsilon(k_i)}{\partial k_i} = v_i. \tag{8.20}$$

Therefore, we find that

$$J_{i,j} = \delta_{ij} v_i, \tag{8.21}$$

and

$$j_\varepsilon = \sum_i v_i |a_i|^2 = 0. \tag{8.22}$$

From Eq. (8.9), we can obtain the total number of states by starting with

$$\langle\varepsilon|\,\hat{j}_\xi \partial_\varepsilon\,|\varepsilon\rangle = i\sum_{l\le x<r} t_{r-l}\Big[e^{ik_i l+ik_j r}\Big(\partial_\varepsilon a_j + \frac{ir}{v_j}a_j\Big) - e^{ik_i r+ik_j l}\Big(\partial_\varepsilon a_j + \frac{il}{v_j}a_j\Big)\Big]\bar{a}_i, \tag{8.23}$$

$$= \bar{a}_i J_{ij}\Big(\partial_\varepsilon a_j + \frac{i\xi}{v_j}a_j\Big) + \delta J_{ij}\bar{a}_i a_j, \tag{8.24}$$

where Eq. (8.24) is obtained by substituting $2r = 2x + 1 + y + d$ into Eq. (8.23) and

$$\delta J_{ij} = -\frac{e^{-i2k_-\xi}}{v_j}\sum_{d,y} t_d\Big[y\sin k_- y\sin k_+ d + \cos k_- y\cos k_+ d\Big] \tag{8.25}$$

and $k_\pm = \frac{1}{2}(k_i \pm k_j)$. The substitution of r leads to the convenient separation of the diagonal term and off-diagonal term given as the first and second term respectively of Eq. (8.24).

Calculating, we find

$$\delta J_{ij} = \begin{cases} i = j, & -\frac{1}{v_i}\sum_d d^2 t_d \cos kd = \frac{1}{2}\partial_\varepsilon v_i \\ i \neq j, & -\frac{1}{2\sin k_-}e^{-2ik_-\xi}. \end{cases} \tag{8.26}$$

Gathering all terms we have

$$\langle\varepsilon|\,\hat{j}_\xi \partial_\varepsilon\,|\varepsilon\rangle = \sum_i \bar{a}_i\Big[i\xi + v_i\partial_\varepsilon + \frac{1}{2}\partial_\varepsilon v_i\Big]a_i - \sum_{i\neq j}\frac{e^{-ik_{ij}\xi}}{2\sin k_{ij}/2}\bar{a}_i a_j, \tag{8.27}$$

where $k_{ij} = k_i - k_j$, $\xi = x + 1/2 \to \infty$.

This diagonal contribution for $a_i = |a_i|e^{i\phi_i}$ becomes

$$\frac{1}{2}\partial_\varepsilon j_\epsilon + i\Big(\xi + v_i\partial_\varepsilon\phi_i\Big)|a_i|^2 = i\Big(\xi + v_i\partial_\varepsilon\phi_i\Big)|a_i|^2 \tag{8.28}$$

since $j_\varepsilon = 0$.

The off-diagonal contribution is important only at the extremal point $v(\varepsilon) = 0$ where degeneracy $k_i(\varepsilon) = k_j(\varepsilon)$ for some i and j. The off-diagonal term is

$$-\frac{1}{2\Delta k_\mu}\Big[e^{-i2\Delta k_\mu\xi}\bar{a}(k_\mu+0)a(k_\mu-0) - e^{i2\Delta k_\mu\xi}\bar{a}(k_\mu-0)a(k_\mu+0)\Big], \tag{8.29}$$

where

$$\Delta k_\mu = \sqrt{2m_\mu|\varepsilon-\varepsilon_\mu|} = k - k_\mu > 0 \quad \varepsilon \approx \varepsilon_\mu \pm \frac{(k-k_\mu)^2}{2m_\mu} \tag{8.30}$$

with mass, m.

There should not be any divergence as $\varepsilon \to \infty$ more than the linear term which has already been obtained in the diagonal contribution. Therefore, the following must hold:

$$\bar{a}(k_\mu+0)a(k_\mu-0) = \bar{a}(k_\mu-0)a(k_\mu+0) = A_\mu. \tag{8.31}$$

This means that A_μ is real, $|a(k)|$ is continuous and $\phi(k)$ jumps as k_μ where $\phi(k)$ is the phase of $a(k)$. The contribution becomes

$$-\frac{\sin 2\Delta k_\mu\varepsilon}{\Delta k_\mu}A_\mu \underset{\varepsilon\to\infty}{\to} -\frac{\pi}{2}\delta(k-k_\mu)A_\mu. \tag{8.32}$$

The extra $\frac{1}{2}$ takes into account that both $k = k_\mu \pm \sqrt{2\omega_\mu|\varepsilon-\varepsilon_\mu|}$ correspond to the same energy ε, and to avoid double counting which k is allowed to be at both sides of k_μ, we need this $\frac{1}{2}$.

The final result for $N_x(\varepsilon) = \langle\varepsilon|\,\hat{N}_x\,|\varepsilon\rangle$:

$$N_x(\varepsilon) = \sum_i (x + \frac{1}{2} + v_i\partial_\varepsilon\phi_i)|a_i|^2 + \frac{\pi}{2}\sum_\mu \delta(k - k_\mu)A_\mu. \tag{8.33}$$

8.2 Quantification of bound states

There is one maximum and one minimum in the 2π interval. Due to TRS, the dispersion $\varepsilon_k = \varepsilon_{-k}$ with periodicity $\varepsilon_{k+2\pi} = \varepsilon_k$, is symmetric (even function) with respect to two inversion centres: $\varepsilon_k = \varepsilon_{-k}$ and $\varepsilon_{k+\pi} = \varepsilon_{\pi-k}$. One maximum and one minimum is only possible for $k_\mu = 0, \pi$. And since we have only two roots of $\varepsilon_k = \varepsilon$, we identify one as incoming and one outgoing momentum.

$$j_\varepsilon = \sum_i v_i|a_i|^2 = |v|[|a_{out}|^2 - \left|a_{in}^2\right|] = 0. \tag{8.34}$$

We can assume that the minimum is at $k = 0$, and the maximum is at $k = \pi$. Integrating over all states we get

$$N_x = \int_{-\pi}^{\pi} \frac{dk}{\pi}[(x + \frac{1}{2} + \partial_k\phi)|a_k|^2 + \frac{\pi}{2}[A_0\delta(k) + A_\pi\delta(k - \pi)]], \tag{8.35}$$

where we used $v_i\partial_\varepsilon = \frac{\partial}{\partial k_i}$.

Since $|a_k|^2 = \frac{1}{2}$ (because $j_\varepsilon = |v|[|a_{out}|^2 - \left|a_{in}^2\right|] = 0$ and due to normalisation $|a_{out}|^2 + \left|a_{in}^2\right| = 1$),

$$N_x = x + \frac{1}{2} + \frac{\Delta\phi}{2\pi} + \frac{1}{2}(A_0 + A_\pi). \tag{8.36}$$

We have

$$A_0 = \bar{a}(+0)a(-0) = \bar{a}(-0)a(+0) = r_0|a_0|^2, \tag{8.37}$$

$$A_\pi = \bar{a}(\pi + 0)a(\pi - 0) = \bar{a}(\pi - 0)a(\pi + 0) = r_\pi|a_\pi|^2 \tag{8.38}$$

with $r_0 = \pm 1$ and $r_\pi = \pm 1$. Finally,

$$-N_b = \frac{1}{2} + \frac{\Delta\phi}{2\pi} + \frac{1}{4}(r_0 + r_\pi). \tag{8.39}$$

$\Delta\phi$ is a change of the smooth part of the function ϕ_k. The total change

$$\Delta_t\phi = \Delta\phi + \sum_\mu \delta_\mu\phi, \quad \delta_\mu\phi = \phi(k_\mu + 0) - \phi(k_\mu - 0) \tag{8.40}$$

is the sum of smooth and jump contributions. And since $r_\mu = e^{i\delta_\mu\phi} = \pm 1$,

$$\delta_\mu\phi = \frac{1 - r_\mu}{2}\pi + 2\pi N_\mu. \tag{8.41}$$

Then:

$$-N_b = \frac{1}{2} + \frac{\Delta_t\phi}{2\pi} - \frac{1}{2\pi}\sum_\mu \Big[\frac{\pi}{2}(1 - r_\mu) + 2\pi N_\mu\Big] + \frac{1}{4}\sum_\mu r_\mu \tag{8.42}$$

$$= \frac{\Delta_t\phi}{2\pi} + \frac{r_0 + r_\pi}{2} - (N_0 + N_\pi). \tag{8.43}$$

Since solutions are periodic with respect to $k \to k + 2\pi$, the total change $\Delta_t\phi = 2\pi/\text{int}$, and $(r_0 + r_\pi)/2 = 0, \pm 1$, we have integer on the RHS.

8.3 Chapter summary

We applied the continuity equation to an infinite system with arbitrary hopping in order to derive the total number of bound states. Using the fact that current in state $|\varepsilon\rangle$ is 0, and the relationship between the total number of states and the current, we explicitly derived the total number of states, $N_x(\varepsilon)$. The degenerate points at $k = 0, \pi$ led to the total number of states depending on a phase and the reflection coefficients. Finally, periodicity allowed us to show that the number of bound states is always an integer.

Chapter 9

Bound states for the SSH model with arbitrary hopping

In this section we calculate the number of bound states for the SSH model with arbitrary hopping as opposed to previous sections in which we focused on nearest-neighbour hopping only.

9.1 The semi-infinite chain

We simplify the model by considering time reversal invariant momenta (or, TRIM) only. This means $\varepsilon_{-k} = \varepsilon_{k+2n\pi}$, and therefore $k = 0, \pi$. The total number of states adapted from Eq. (8.33) is

$$N_x^{\varepsilon} = \sum_i \Big(x + \frac{1}{2} + v_i \partial_{\varepsilon} \phi_k |a_i|^2 + \frac{\pi}{2} \sum_{\mu} \delta_{\mu} r_{\mu} |a_{\mu}|^2 \Big). \tag{9.1}$$

Since a wavefunction is defined up to a phase, we can always choose $a_{k<0}$ real,

$$a_{k<0} = \frac{1}{\sqrt{2}}, \quad a_{k>0} = \frac{e^{i\phi_k^r}}{\sqrt{2}} = \frac{r_k}{\sqrt{2}}. \tag{9.2}$$

Then

$$N_x^{\varepsilon} = x + \frac{1}{2} + \frac{1}{2} v \partial_{\varepsilon} \phi_k^r + \frac{\pi}{4} \sum_{\mu} \delta_{\mu} r_{\mu}, \tag{9.3}$$

and

$$N_x = \int_0^{\pi} \frac{dk}{\pi} N_x^{\varepsilon} = x + \frac{1}{2} + \frac{\Delta\phi_r}{2\pi} + \frac{1}{4} \sum_{\mu} r_{\mu}, \tag{9.4}$$

where

$$\Delta\phi_{\mu}^r = \phi_{\mu+0}^r - \phi_{\mu-0}^r, \quad r_{\mu} = e^{i\Delta\phi_{\mu}} = \pm 1, \tag{9.5}$$

$$\Delta\phi_{\mu}^r = \begin{cases} \Delta\phi_0^r = & \phi_{k=+0}^r - \phi_{k=-0}^r \\ \Delta\phi_{\pi}^r & \phi_{k=\pi+0}^r - \phi_{k=\pi-0}^r \end{cases} \tag{9.6}$$

and since

$$a_{k+2\pi} = a_k \implies e^{i\Delta\phi_r} = r_0 r_{\pi}. \tag{9.7}$$

$$r_0 r_{\pi} = 1, \quad \implies \Delta\phi_r = 2n\pi \quad \implies -N_b = \frac{\Delta\phi_r}{2\pi} + \frac{1+\rho}{2} = \text{int}, \tag{9.8}$$

since $r_0 = r_{\pi} = \rho = \pm 1$.

$$r_0 r_{\pi} = -1 \quad \implies \Delta\phi_r = (2n+1)\pi \quad \implies -N_b = \frac{\Delta\phi_r}{2\pi} + \frac{1}{2} = \text{int}. \tag{9.9}$$

This is similar to the result for topological insulators:

$$r_{\mu} = \pm 1 \implies \psi_x^{\mu} \to \begin{cases} \cos k_{\mu} x \\ \\ \sin k_{\mu} x \end{cases}, \tag{9.10}$$

where μ is analogous to ε_k for odd/even parities in the case of topological insulators.

9.2 The infinite chain

For an infinite chain, waves can propagate towards $\pm\infty$, contrary to a semi-infinite system which is only half of the picture. In this case, we must consider scattering amplitudes for

both sides of the origin. The total number of states for an infinite system

$$\hat{N}_{xx'} = \sum_{x'<S\leq x} |s,\alpha\rangle \langle s,\alpha| \tag{9.11}$$

where α is the index for left and right incoming waves. Adapting from the semi-infinite system we have

$$N_x^{\varepsilon} = \sum_{\alpha} = \langle \varepsilon,\alpha| \hat{N}_{xx'} |\varepsilon,\alpha\rangle = -i \sum_{\alpha} \Big(\langle \varepsilon,\alpha| \hat{j}_{x+\frac{1}{2}} |\varepsilon,\alpha\rangle - \langle \varepsilon,\alpha| \hat{j}_{x'+\frac{1}{2}} |\varepsilon,\alpha\rangle \Big). \tag{9.12}$$

Using the previously derived scattering matrix for this system,

$$\hat{S} = \begin{pmatrix} r & t \\ t & r \end{pmatrix}, \quad \hat{S}\hat{S}^{\dagger} = 1, \quad \hat{S} = \hat{S}^{T}(\text{TRS}), \tag{9.13}$$

$$N_{xx'}^{\varepsilon} = 2(x-x') + v\Big[\partial_{\varepsilon}(\phi_r + \phi_{r'})R + 2\partial_{\varepsilon}\phi_t T\Big] + \frac{\pi}{2}\sum_{\mu}\delta_{\mu}(r_{\mu} + r'_{\mu}) \tag{9.14}$$

$$= 2(x-x') - iv\,\mathrm{tr}\,\hat{S}^{\dagger}\partial_{\varepsilon}\hat{S} + \frac{\pi}{2}\sum_{\mu}\delta_{\mu}(r_{\mu} + r'_{\mu}) \tag{9.15}$$

$$= 2(x-x') + v\partial_{\varepsilon}\chi + \frac{\pi}{2}\sum_{\mu}\delta_{\mu}(r_{\mu} + r'_{\mu}), \tag{9.16}$$

where $\det \hat{S} = e^{i\chi}$. The excess density of states is

$$\delta\nu_{\varepsilon} = v\partial_{\varepsilon}\chi = \partial_k\chi \quad \text{for } \varepsilon_{\min} < \varepsilon < \varepsilon_{\max}. \tag{9.17}$$

The excess charge, or $-N_b$:

$$-N_b = \int_0^{\pi} \frac{dk}{2\pi}\delta\nu_{\varepsilon} = \frac{\Delta\chi}{2\pi} + \frac{1}{4}\sum_{\mu}\delta_{\mu}(r_{\mu} + r'_{\mu}). \tag{9.18}$$

Taking into account the periodicity in k-space, we have

$$e^{i\Delta\chi} = r_0 r_\pi r_0' r_\pi' \Big(\equiv \prod_{\mu=1}^{k} r_\mu \Big) \tag{9.19}$$

$$\prod_{\mu=1}^{k} r_\mu = 1 \implies \Delta\chi = 2n\pi, \tag{9.20}$$

$$\prod_{\mu=1}^{k} r_\mu = -1 \implies \Delta\chi = (2n+1)\pi. \tag{9.21}$$

9.3 The SSH model

The solution

$$\vec{\psi}_x^{\varepsilon} = \vec{a}_k e^{ikx} + \vec{a}_{-k} e^{-ikx} \quad \text{for } \vec{\psi}_x = \begin{pmatrix} A_x \\ B_{x+\frac{1}{2}}, \end{pmatrix} \tag{9.22}$$

where A-sites are labelled by an integer x, and B-sites are sitting at half-integers. This notation is used to keep $x \to x+1$ periodicity and, hence, $k \to k+2\pi$ periodicity.

Our results for the total number of sites are easily generalised for $a_i \to \vec{a}_i$:

$$N_x^{\varepsilon} = (x + \frac{1}{2}) \sum_i \vec{a}_i^{\dagger} \vec{a}_i + \sum_i \frac{\partial \phi_i}{\partial k_i} \vec{a}_i^{\dagger} \vec{a}_i + \frac{\pi}{2} \sum_\mu r_\mu \vec{a}_\mu^{\dagger} \vec{a}_\mu. \tag{9.23}$$

Like before, we assume that we have only two solutions $\varepsilon(k) = \varepsilon$, and as a result, only two zero-velocity momenta 0 and π. Vectors $\vec{a}_i = \vec{a}(k = k_i(\varepsilon)) = \vec{a}_{k=k_i(\varepsilon)}$ are solutions of

$$\hat{h}_k \vec{a}_k = \varepsilon_k \vec{a}_k, \quad \hat{h}_k = \begin{pmatrix} 0 & -\tau_k \\ -\bar{\tau}_k & 0 \end{pmatrix}, \quad \tau_k = \tau e^{ik/2} + e^{-ik/2}, \quad \varepsilon_k^2 = |\tau_k|^2. \tag{9.24}$$

Integrating

$$N_x = \int_0^{\pi} \frac{dk}{\pi} N_x^{\varepsilon_k}, \tag{9.25}$$

and summing over two bands,

$$N_x = 2\Big(x+\frac{1}{2}\Big) + \int \frac{dk}{2\pi}\partial_k\Big(\phi_k^+\phi_k^-\Big) + \frac{1}{4}\sum_\mu \delta_\mu(r_\mu + r'_\mu), \tag{9.26}$$

$$= 2x + 1 + \frac{\Delta\phi^+ + \Delta\phi^-}{2\pi} + \frac{1}{4}\sum_\mu \delta_\mu(r_\mu + r'_\mu). \tag{9.27}$$

Here $\phi^\pm$ are phases $\vec{a_k}^\pm$:

$$\vec{a_k}^\pm = a_k^\pm \vec{U}_k^\pm, \quad \vec{U}_k^\pm = \frac{1}{\sqrt{2}}\begin{pmatrix} e^{i\theta_k} \\ \mp 1 \end{pmatrix}, \tag{9.28}$$

where

$$a_k^\pm = |a_k^\pm| e^{i\chi_k^\pm} = \frac{1}{\sqrt{2}} e^{i\chi_k^\pm}, \quad \tau_k = |\tau_k| e^{i\theta_k}, \quad \phi_k^\pm = \chi_k^\pm + \theta_k. \tag{9.29}$$

$$-N_b = 1 + \frac{\Delta\phi^+ + \Delta\phi^-}{2\pi} + \frac{1}{4}(r_0^+ + r_\pi^+ + r_0^- + r_\pi^-), \tag{9.30}$$

where $r_\mu^\pm$ are reflection amplitudes in upper $(+)$ and lower $(-)$ bands.

The total excess can be written as

$$+N_b = +N_b^+ + N_b^- - \frac{\Delta\theta}{\pi}, \tag{9.31}$$

where

$$N_b^\pm = \frac{1}{2} + \frac{\Delta\chi^\pm}{2\pi} + \frac{1}{4}(r_0^\pm + r_\pi^\pm) \tag{9.32}$$

are contributions from the reflection amplitudes including phase and coefficients at 0 and π. This is considered non-universal since it depends on the type of disorder present in the system. The $\frac{-\Delta\theta}{\pi}$ term in Eq. (9.31)is the universal additional contribution arising from the spinor $\vec{U}_k^\pm$ which is defined far from the origin and depends on the bulk solution only.

Since $\vec{a}_{k+2\pi} = \vec{a}_k$,

$$\vec{a}_{k+2\pi} = \begin{pmatrix} r_0^+ r_\pi^+ e^{i\Delta\chi^+} & 0 \\ 0 & r_0^- r_\pi^- e^{i\Delta\chi^-} \end{pmatrix} (-\hat{\sigma}_3)\vec{a}_k = \pm\vec{a}_k. \tag{9.33}$$

Therefore, $r_0^\pm r_\pi^\pm e^{i\Delta\chi^\pm} = \pm 1$ for both bands. Finally, the phase of the reflection coefficients are

$$e^{i\Delta\chi^\pm} = \pm r_0^\pm r_\pi^\pm \implies \Delta\chi^\pm = \begin{cases} 2n\pi \\ (2n+1)\pi, \end{cases} \tag{9.34}$$

depending on $r_\mu^\pm$.

9.4 Chapter summary

We observed that the total number of bound states for an infinite SSH chain depended on the change of two phases. Since the total number of states must be an integer, we find that these two phases are also integers. The bulk solutions located far from the origin led to spinors with a universal phase, $\Delta\theta/\pi$. The reflection amplitudes however, led to the phase $\Delta\chi^\pm/2\pi$ which depended on the disorder located at the origin, and therefore was identified as non-universal.

Chapter 10

Strongly correlated 1D systems: The Sliding Luttinger Liquid

In this section we will consider a system of parallel quantum wires separated by gaps of alternating size. Since quantum wires are an example of a one-dimensional conductor, we use the Luttinger Liquid model to describe interacting fermions within each wire. The system is constructed in analogy of the one-dimensional SSH model, however, we also introduce interwire interaction due to the multi-wire construction. Therefore, the system will have a total of two dimensions, one being the intrawire interaction between particles and the other being interwire interaction. This added feature of interwire interaction leads to the sliding effect such that the electronic movement within one wire affects those that are in coupled neighbouring wires. This is referred to as the sliding Luttinger liquid (SLL) phase. However, due to coupling between the wires the SLL phase can be unstable. The charge-density wave (CDW) perturbation occurs when electrons collectively move carrying charge in wave-like behaviour. This charge density can be modulated resulting in periodic distortion, or 'bumps' of charge and therefore, is one such source of instability of the SLL phase. Another is the superconducting (SC) phase due to the interwire interaction. In this phase charge moves completely free with zero resistance.

In the following sections, we analyse the parameters under which these two phases destabilise the SLL phase. We define the Luttinger matrix, $\hat{K}$ which we use to express the scaling dimensions of both CDW and SC phases. These scaling dimensions are then used to map out a stability region for the SLL phase.

10.1 The Luttinger model

In the following analysis, we once again consider the motion of electrons as quasi-particles since Luttinger bosons cannot tunnel between chains. This is because we consider a spin-gapped system where spin degrees of freedom are suppressed, and therefore, single particle tunnelling is also suppressed. The system of N parallel quantum wires can be described by the standard bosonized Lagrangian

$$L = \frac{1}{4\pi}\left[\partial_t\varphi\partial_x\theta + \frac{1}{2}\partial_x\theta^T V_\theta \partial_x\theta + \frac{1}{2}\partial_x\varphi^T V_\varphi \partial_x\varphi\right] \tag{10.1}$$

where $\theta = \{\theta_1, \theta_2, ..., \theta_N\}$ and $\varphi = \{\varphi_1, \varphi_2, ..., \varphi_N\}$ are fields which represent the current $j_i = \frac{1}{\pi}\partial_x\theta_i$ and density $\delta\rho_i = \frac{1}{\pi}\partial_x\varphi_i$ fluctuations. The matrices $\hat{V}_\varphi$ and $\hat{V}_\theta$ are tri-diagonal. We will only analyze the commonly accepted model that includes only a density-density interaction, therefore, the current-current interaction $\hat{V}_\theta = \mathbb{1}$ in Eq. (10.1). As a result, the density-density interaction matrix takes the form,

$$\hat{V}_\phi = \begin{bmatrix} 1+g & g_o & 0 & 0 & \dots & 0 & 0 \\ g_0 & 1+g & g_e & 0 & \dots & 0 & 0 \\ 0 & g_e & 1+g & g_e & \dots & 0 & 0 \\ 0 & 0 & g_o & 1+g & \dots & 0 & 0 \\ \dots & \dots & \dots & \dots & \dots & \dots & \dots \\ 0 & 0 & 0 & 0 & \dots & g_o & 1+g \end{bmatrix} \tag{10.2}$$

with $g = 2\pi(g_4 + g_2)$ where g_4 and g_2 are forward and back scattering amplitudes. In

the off diagonal entries, g_o and g_e are labels to differentiate between wires that follow gaps of different size.

It is convenient to define a Luttinger matrix $\hat{K}$ which is a generalisation of the Luttinger parameter K of a single channel, independent of the number i of the wire, i.e. all the wires are identical. All scaling dimensions can be expressed using this single matrix $\hat{K}$ since it provides information on the relevance of the perturbations, and therefore on the stability of the region of the SLL phase. In this case, the $\hat{K}$ matrix is the solution of the matrix equation $\hat{K}\hat{V}_\phi\hat{K} = \hat{\mathbb{1}}$, i.e. the square root of the interaction matrix $\hat{K} = \hat{V_\phi}^{-1/2}$.

10.2 Eigenfunctions of the interaction matrix

In order to find $\hat{K}$ we need to know the eigenvalues λ and eigenvectors ψ of the matrix $\hat{V}_\phi$. We repeat identical steps from chapter 5 and therefore omit repeated explanation where it is unnecessary. We can imagine two groups of wires, one with M even wires only and the other with $M+1$ odd wires only, resulting in a total of $2M+1$ wires. Then the eigenfunctions are,

$$g_o\psi_{2j-1} + g_e\psi_{2j+1} = \varepsilon\psi_{2j}, \quad j = 1, ..., M \tag{10.3}$$

$$g_e\psi_{2j-2} + g_o\psi_{2j} = \varepsilon\psi_{2j-1}, \quad j = 1, ..., M+1 \tag{10.4}$$

where we define $\varepsilon = \lambda - (1+g)$. To create a finite system the boundary condition is imposed

$$\psi_0 = \psi_{2M+2} = 0 \tag{10.5}$$

and acts on the second eigenfunction. The edge states developing at the edge of the system could be governed by open boundary conditions, much like the standard SSH model under standard conditions. We are concerned with the bulk states of this system and we will later show that the presence of edge states does not effect the bulk properties of a couple chained

model. We find eigenfunctions

$$\psi_{k,2j} = e_k e^{ikj} + e_{-k} e^{-ikj} \tag{10.6}$$

$$\psi_{k,2j-1} = o_k e^{ikj} + o_{-k} e^{-ikj}, \tag{10.7}$$

where k is the wave vector and the coefficients e_k and o_k satisfy

$$g_k o_k = \varepsilon_k e_k \tag{10.8}$$

$$\bar{g_k} e_k = \varepsilon_k o_k, \tag{10.9}$$

with $g_k = g_o + g_e e^{ik} = |g_k| e^{i\phi_k}$.

Using these equation we find eigenenergies ε_k

$$\varepsilon_{\pm k} = \pm |g_k|. \tag{10.10}$$

Inserting the boundary condition $\psi(0) = 0$ into Eq. (10.6) we obtain:

$$e_{-k} = -e_k. \tag{10.11}$$

The normalised bulk states obtained using Eq. (10.11)

$$\psi^b_{\pm k,2j} = \frac{1}{\sqrt{M+1}} \sin kj, \tag{10.12}$$

$$\psi^b_{\pm k,2j-1} = \pm \frac{1}{\sqrt{M+1}} \sin(kj - \phi_k), \tag{10.13}$$

with k quantised to be

$$k = \frac{\pi n}{M+1}, \quad n = 1, ..., M. \tag{10.14}$$

due to the second boundary condition $\psi_{2M+2} = 0$.

There are therefore $2M$ bulk solutions labelled by k and one more solution at $\varepsilon = 0$, since there are $2M + 1$ solutions all-together. We identify this as an edge state which is localised at the left boundary

$$\psi^e_{2j-1} = N_0\Big(-\frac{g_o}{g_e}\Big)^j, \quad \psi^e_{2j} = 0, \quad N^0 = \Big[\frac{(-\frac{g_o}{g_e})^2 - (-\frac{g_o}{g_e})^{2(M+2)}}{1-(-\frac{g_o}{g_e})^2}\Big]^{-1/2}. \tag{10.15}$$

When $g_0 < g_e$ the edge state is exponentially localised at the left boundary, and if $g_o > g_e$ the edge state is exponentially localised at the right boundary.

As mentioned previously $\hat{K} = \hat{V}_\theta^{-1/2}$. The diagonalization of the interaction matrix allows us to obtain the Luttinger matrix in the form

$$\hat{K}_{ij} = K[\sum_{k,\sigma=\pm} \Lambda^{-1/2}_{k,\sigma}\psi^\sigma_k(i)\psi^\sigma_k(j) + \psi_0(i)\psi_0(j)] \tag{10.16}$$

where we used the eigenvalues

$$\lambda_{k,\pm} = \frac{1}{K^2}\Lambda_{k,\pm} = \pm|g_k| + 1 + g \tag{10.17}$$

and

$$\lambda_0 = 1 + g \equiv K^{-2}, \tag{10.18}$$

and the corresponding eigenvectors $\psi^\pm_k(i)$ and $\psi_0(i)$.

We can write the equation for the inverse Luttinger liquid matrix

$$(\hat{K}^{-1})_{ij} = K[\sum_{k,\sigma=\pm} \Lambda^{1/2}_{k,\sigma}\psi^\sigma_k(i)\psi^\sigma_k(j) + \psi_0(i)\psi_0(j)]. \tag{10.19}$$

We are trying to identify the case when the SLL phase is stable with respect to two processes: formation of CDW and SC states. In order to do this, we must ensure that the relevant

processes are RG irrelevant. The scaling dimensions of couplings between wires i and j are

$$\Delta_{ij}^{CDW} = \hat{K}_{ii} + \hat{K}_{jj} - 2\hat{K}_{ij} \tag{10.20}$$

and

$$\Delta_{ij}^{SC} = (\hat{K}^{-1})_{ii} + (\hat{K}^{-1})_{jj} - 2(\hat{K}^{-1})_{ij} \tag{10.21}$$

for the processes responsible for the CDW and SC phases formation respectively. We will only consider the most dangerous among them, corresponding to neighbouring wires, so that $j = i + 1$.

10.3 Bulk scaling dimensions

To obtain the scaling dimensions for each perturbation, we first substitute the known eigenvalues and eigenfunctions into Eq.'s (10.16) and (10.19) to obtain $\hat{K}$ values and then into Eq.'s (10.20) and (10.21). This leads to two CDW scaling dimensions given as

$$\Delta_e^{CDW} = 2K \int_0^{\pi} \frac{dk}{\pi} \left[\lambda_+^{-\frac{1}{2}} \sin^2 \frac{\phi}{2} + \lambda_-^{-\frac{1}{2}} \cos^2 \frac{\phi}{2} \right] \tag{10.22}$$

$$\Delta_o^{CDW} = 2K \int_0^{\pi} \frac{dk}{\pi} \left[\lambda_+^{-\frac{1}{2}} \sin^2 \frac{\phi - k}{2} + \lambda_-^{-\frac{1}{2}} \cos^2 \frac{\phi - k}{2} \right] \tag{10.23}$$

and similarly two SC scaling dimensions given as

$$\Delta_e^{SC} = 2K \int_0^{\pi} \frac{dk}{\pi} \left[\lambda_+^{\frac{1}{2}} \sin^2 \frac{\phi}{2} + \lambda_-^{\frac{1}{2}} \cos^2 \frac{\phi}{2} \right] \tag{10.24}$$

$$\Delta_o^{SC} = 2K \int_0^{\pi} \frac{dk}{\pi} \left[\lambda_+^{\frac{1}{2}} \sin^2 \frac{\phi - k}{2} + \lambda_-^{\frac{1}{2}} \cos^2 \frac{\phi - k}{2} \right] \tag{10.25}$$

These equations for the scaling dimensions are located in the bulk far from the edges in the limit $M \to \infty$. Since we have two wires, odd and even, we also have two eigenfunctions leading to two CDW scaling dimensions and SC dimensions.

For convenience, we will now introduce two inter-channel parameters (instead of $g_{o,e} = \tilde{g} \pm \Delta$) $\alpha = \frac{2\tilde{g}}{1+g}$ and $\beta = \frac{\Delta}{\tilde{g}}$, where α is the relative strength of the inter-channel interaction and β is the relative strength of asymmetry, or modulation. The Luttinger parameter, K and α can both vary between 0 and 1. Although in principle, β varies between -1 and 1, due to the symmetry below we can see that the range can also be reduced to 0 and 1. Now we can introduce the relations

$$\lambda_k^{\pm} = 1 \pm \alpha \sqrt{\cos^2 \frac{k}{2} + \beta^2 \sin^2 \frac{k}{2}} \tag{10.26}$$

$$\cos \phi_k = \frac{\cos^2 \frac{k}{2} - \beta \sin^2 \frac{k}{2}}{\sqrt{\cos^2 \frac{k}{2} + \beta^2 \sin^2 \frac{k}{2}}}$$

$$\cos(\phi_k - k) = \frac{\cos^2 \frac{k}{2} + \beta \sin^2 \frac{k}{2}}{\sqrt{\cos^2 \frac{k}{2} + \beta^2 \sin^2 \frac{k}{2}}}$$

$$\sin \phi_k = \frac{\cos \frac{k}{2} \sin \frac{k}{2}(1+\beta)}{\sqrt{\cos^2 \frac{k}{2} + \beta^2 \sin^2 \frac{k}{2}}} \tag{10.27}$$

From each pair of scaling dimensions, we choose only the more dangerous to obtain results for K_{CDW}^{-1} and K_{SC}. We observe that due to the inequalities: $\lambda_k^+ > \lambda_k^-$ and $\cos(\phi_k - k) > \cos(\phi_k)$, Eq.'s (10.22) and (10.25) are more dangerous (smaller) for $\beta > 0$ and therefore, must be considered. As a result, we obtain equations for the scaling dimensions which are even in β, allowing it to be sufficient to consider β varying between 0 and 1. Finally, we represent scaling dimensions in the form

$$\Delta_{CDW} = 2\frac{K}{K_{CDW}(\alpha, \beta)}, \ \Delta_{SC} = 2\frac{K_{SC}(\alpha, \beta)}{K} \tag{10.28}$$

$$CDW = R_i^\dagger L_i \cdot L_j^\dagger R_j, \qquad SC = R_i L_i \cdot R_j^\dagger L_j^\dagger$$

$$K_{CDW}^{-1} = \int_0^{\frac{\pi}{2}} \frac{dk}{\pi} \left[\frac{1}{\sqrt{1+\alpha r}} \left(1 - \frac{\cos^2 k - |\beta| \sin^2 k}{r} \right) + \frac{1}{\sqrt{1-\alpha r}} \left(1 + \frac{\cos^2 k - |\beta| \sin^2 k}{r} \right) \right] \quad (10.29)$$

$$K_{SC} = \int_0^{\frac{\pi}{2}} \frac{dk}{\pi} \left[\frac{1}{\sqrt{1+\alpha r}} \left(1 - \frac{\cos^2 k + |\beta| \sin^2 k}{r} \right) + \frac{1}{\sqrt{1-\alpha r}} \left(1 + \frac{\cos^2 k + |\beta| \sin^2 k}{r} \right) \right] \quad (10.30)$$

where $r = \sqrt{\cos^2 k + \beta^2 \sin^2 k}$.

10.4 Stability region of the SLL phase

The scaling dimensions Eq. (10.28) for CDW and SC phases are RG irrelevant if both are larger than 2. It therefore must be that the intrawire Luttinger parameter K satisfies the condition

$$K_{SC} > K > K_{CDW}. \quad (10.31)$$

It follows that the above inequality can be satisfied if the product of integrals defined in Eq.'s (10.29) and (10.30) is greater than 1:

$$\prod \equiv K_{SC} K_{CDW}^{-1} > 1. \quad (10.32)$$

The inequality (10.31) allows us to easily find the stability region of the SLL phase.

Fig. 10.1 shows the product of the integrals Eq. (10.32) in 3D as a function of the two parameters α and β. In addition, a plane is drawn on top to show where the product exceeds

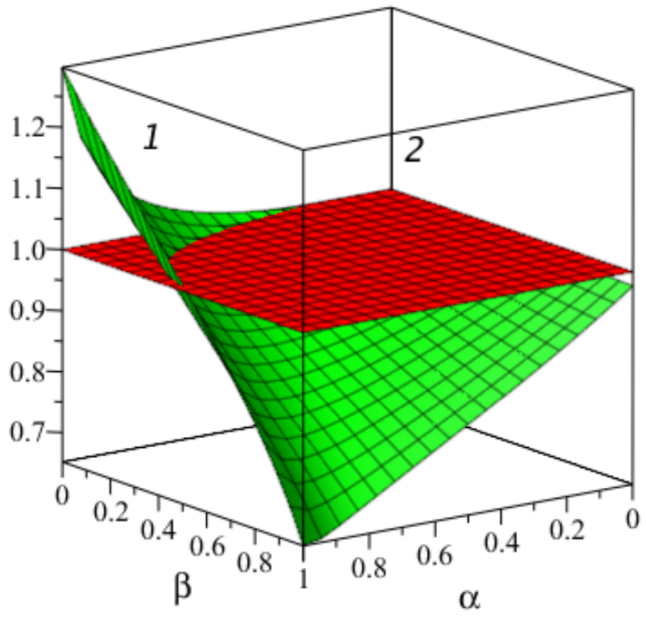

Figure 10.1: A 3D plot of the product Eq. (10.32), labelled 1 crossed by the flat surface labelled 2.

1. As we can see in the $\alpha - \beta$ plane, the section above 1 shows the area where K values satisfying the inequality Eq. (10.32) can be found. At these values of (α, β), we can find the value of K such that both processes CDW and SC are RG irrelevant and the SLL phase is stable. Fig. 10.2 shows this area from a view from above.

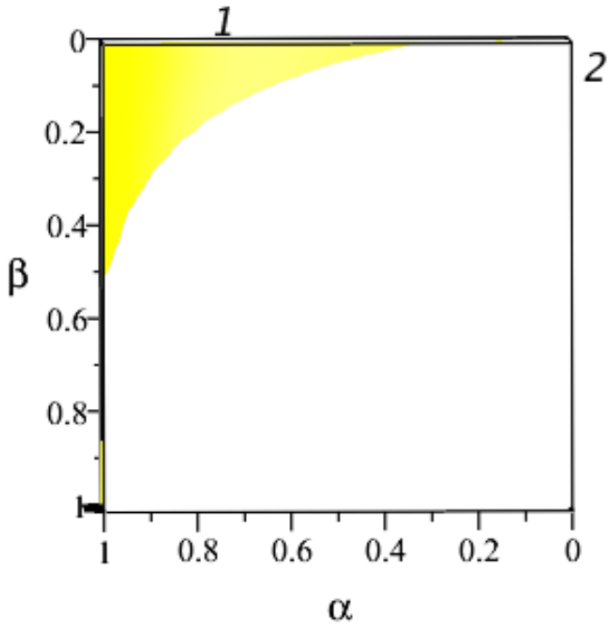

Figure 10.2: A 3D plot of the product Eq. (10.32) crossed by the flat surface labelled 1 and 2 respectively - as seen from above. The region of stability of the SLL phase is clearly seen.

We can see that the stability regions (shaded) is roughly a right-angled triangle with catheti of approximately 0.5 along both α and β axes. In order to estimate the values of which the Luttinger parameter K ensures that the SLL phase remains stable with respect to the formation of CDW and SC phases, we can also plot $K^{-1}_{CDW}(\alpha, \beta)$ and $K_{SC}(\alpha, \beta)$ against one another shown in Fig. 10.3.

The inequality (10.31) can be satisfied if the surface 1 ($K_{SC}(\alpha, \beta)$) lies above the surface 2 $K^{-1}_{CDW}(\alpha, \beta)$, and the desirable K values lie in-between these two surfaces. One can see from Fig. 10.3 that the maximal span from 0.5 to 0.65 of the allowed K values is at $\alpha = 1$ and

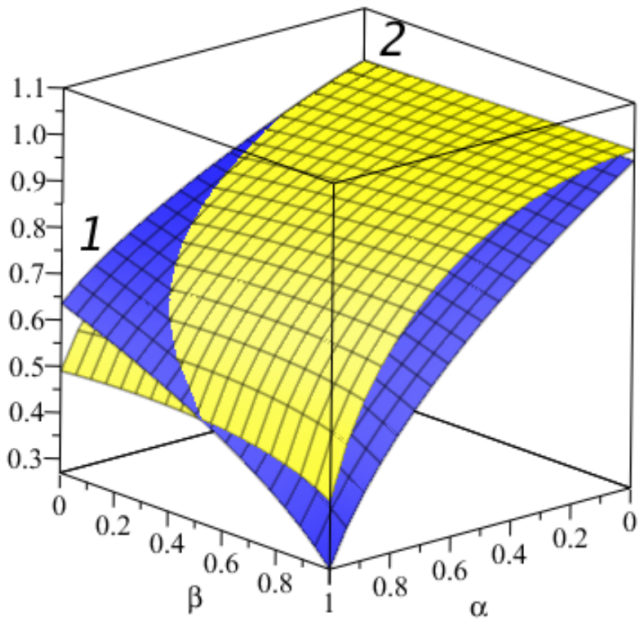

Figure 10.3: A 3D plot of the functions $K_{SC}(\alpha,\beta)$ and $K_{CDW}^{-1}(\alpha,\beta)$ labelled by 1 and 2 respectively.

$\beta = 0$. Then the span gradually narrows and goes to 0 with the increasing β or decreasing α.

The inverse of the inequality Eq. (10.31) can give us the counter perspective, when the CDW and SC perturbations are relevant. We can see that $K_{SC}(\alpha,\beta)$ and $K_{CDW}^{-1}(\alpha,\beta)$ are both equal to 1 at $\alpha = 0$, i.e. $\prod = 1$. This means that the span of allowed values of K reduces to 0 and the SLL phase is marginally stable only in the point $K = 1$. There is a stripe of stability going from the stability triangle along the α axis up to this point. The stripe cannot be seen in Figs. 10.1 and 10.2 since it is so narrow. On the other hand Eq. (10.30) diverges at $\alpha \to 1$. This shows that there is also a very narrow stripe of stability parallel to the β axis along $\alpha = 1$. This behaviour can be illustrated by plotting the characteristic product $\prod$ as a function of of α in Fig. 10.4.

The curve labelled 1 corresponds to $\beta = 0$ and is always greater than 1. This curve grows slowly within the stability stripe and then more rapidly after reaching the triangle before diverging at $\alpha \to 1$. At $\beta = 0.3$ the curve labelled 2 first goes down below 1 (instability) and

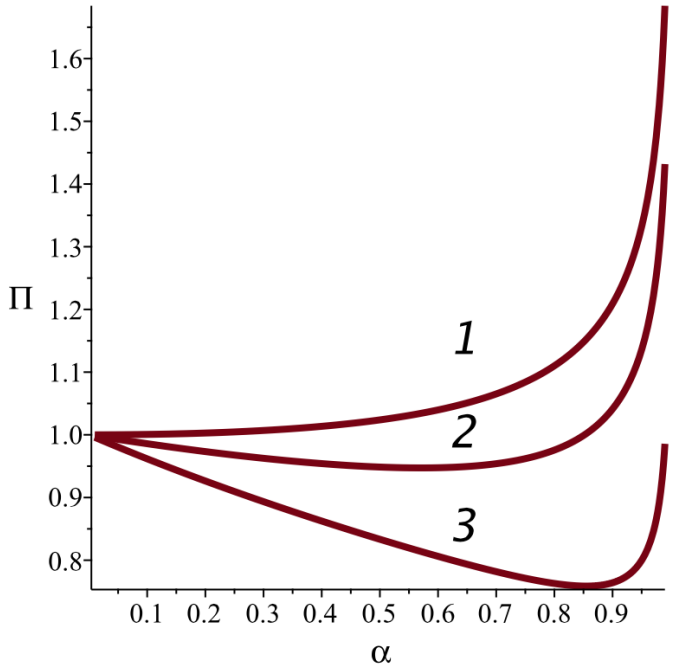

Figure 10.4: The plot of the product $\prod$ as a function of the parameter α for three values of the modulation parameter β; (1)-$\beta = 0$, (2)-$\beta = 0.3$ and (3)-$\beta = 0.8$.

only at $\alpha = 0.85$ crosses the level 1.0 and enters the stability region. At most $\beta = 0.8$ the SLL phase is almost always unstable, except for a narrow region at $\alpha \to 1$. The limit $|\beta| = 1$ describes a system with either g_e or g_o being equal to zero. In this case, our system changes into an array of pairs of quantum wires, decoupled with one another, but coupled within each pair.

10.5 Chapter summary

We showed that there was an edge state localised on the left boundary when $g_o < g_e$, and moved to the right when this ratio was flipped. The Luttinger matrix allowed us to present the relevant scaling dimensions for the CDW and SC perturbations. We showed that the stability region for the SLL phase depended on inter-channel parameters α, β and the Luttinger parameter K. The widest stability region is demonstrated to exist for strong coupling α, weak modulation β and Luttinger parameter $K \in [0.5 - 0.6]$.

Chapter 11

Conclusions and Future work

11.1 The non-interacting model

To summarise, in section 4 we studied the SSH model since it's the simplest non-trivial topological model. We found that the ratio between hopping parameters t_1 and t_2 determined when a gap-less system may occur. No sign of topology could be observed when $t_1 < t_2$ or $t_1 > t_2$, it was specifically at $t_1 = t_2$ that the bands touched, indicating that this was a critical point demonstrating the topological transition through the winding number. This was confirmed in section 4.2 when the topological transition was observed. We saw that when $t_1 > t_2$, t_k did not enclose the origin resulting in a trivial winding number of 0. However, when $t_1 = t_2$ we saw that t_k touched the origin, and when $t_1 < t_2$ it enclosed the origin resulting in a topologically non-trivial number of 1. The Zak-phase coincided with this result since we found that $\phi = 2\pi$ when $\nu = 1$ and 0 otherwise.

We then proceeded to construct edge states for a chain with an odd number of sites. The boundary condition that the wave-function should disappear at the nearest site outside the chain, $\psi_{2M+2} = 0$ led to the quantisation of the wave vector k from which we found $2M$ bulk solutions. Since we initially started with $2M + 1$ degrees of freedom, we can infer that the missing solution is not present in the bulk but the edge instead - an edge state. We solve for the edge state by taking $\varepsilon = 0$ and setting $\psi_{2j} = 0$. We found that the ratio $t_1 < t_2$ played a significant role in the localisation of the edge state. When $t_1 < t_2$, the edge state

is exponentially localised at the left boundary, and if $t_1 > t_2$ the edge state is exponentially localised at the right boundary instead. Therefore we were able to explicitly define the edge state in the case of a chain of an odd number of sites.

Section 5 continued the discussion of special states for the SSH model focusing on scattering amplitudes as opposed to calculating the Zak phase to find the edge states. Here, we instead derive the scattering amplitudes of waves reflecting off a potential centred on an infinite chain. We did this first for a one-dimensional continuous chain with a δ-function potential. We found exponentially decaying bound states localised on either side of the potential. We then proceeded to find the total charge of the same system which we found to be 0 in the presence of the bound state and -1 otherwise. These steps were taken to devise the protocol for the one-dimensional SSH lattice, therefore, we then had to adapt our continuous model to a one-dimensional simple lattice before moving to the SSH lattice. We defined λ as the amplitude to the δ-function potential and found that the sign of λ determined the presence of the bound state. There were two poles found of reflection amplitude, r_k depending on the sign of λ. In the case that $\lambda > 0$ we found oscillating states on either side of the potential and identified these as scattering states. In contrast, when $\lambda < 0$, we found purely exponentially decaying states on either side of the potential and identified this as a bound state. This was supported by applying the one-dimensional Levinson's theorem which uses the phase of the transmission amplitude to determine the number of bound states, which was found to be 1. These steps were then repeated for the SSH model where we similarly found one bound state using the Levinson's theorem.

We then considered two different approaches to calculate the number of bound states in sections 6 and 7. In the first approach, the density of states was calculated in terms of Green's functions leading to the explicit derivation of the s-matrix elements, namely; the reflection and transmission amplitudes of the system. Thus, we found the relationship between the density of states and the s-matrix. For the other approach, we used the continuity equation

to find the density of states. Applying the sum rule, we obtained the number of bound states given in terms of reflection amplitude and the phase of the transmission amplitude. We then tested this on the continuous Schrödinger equation with a δ-function potential and found that the number of bound states is 1 if the amplitude $\lambda = \pm 1$.

In chapters 8 and 9, we studied bound states for systems with arbitrary hopping as opposed to nearest-neighbour hopping, which we previously discussed. We did this by once again exploiting the continuity equation and found the total number of states for first the Bravais lattice, and then the SSH lattice. The number of bound states is found to be exactly an integer and depends on the reflection coefficient at degenerate points $k = 0, \pi$ and the total phase. For the SSH, we first began with a semi-infinite chain showing similar results to that of a Bravais lattice. The reflection coefficient took values $r_\mu = \pm 1$ which showed similarities to the case of topological insulators, and therefore suggests non-trivial behaviour. For an infinite chain, we derived the number of bound states once again depending on the reflection coefficient at $k = 0, \pi$, only there were two bands arising due the spinor involved in the SSH model. There was also a phase which also depended on the reflection coefficient. All terms depending on the reflection coefficient were identified to be non-universal since they were uniquely defined by the disorder placed at the origin. The number of bound states also contained another phase term which came from bulk solutions, and therefore was identified as the universal contribution.

11.2 The interacting model

We discussed the interacting model in section 10 in which we studied the sliding Luttinger liquid. We investigated the stability conditions of the SLL phase in a 2D system of parallel quantum wires with alternating coupling between nearest neighbor wires. We took the density–density interaction into account as the principle coupling mechanism between the wires and neglected the current–current interaction. We analysed the CDW and SC perturbations

with respect to their affect on the stability of the SLL phase. We introduced a Luttinger parameter, K, an interwire coupling strength parameter, α and a modulation strength parameter, β all between 0 and 1 to represent these perturbations. Using re-normalisation group analysis, we presented an analytical derivation of the CDW and SC scaling dimensions. We obtained four scaling dimensions in total; an odd and an even for both perturbations. This occurred due to the odd/even label given to distinguish the wires, which consequently led to an odd/even wave-function for each perturbation. We chose the most dangerous of the scaling dimensions for each case, i.e. $\Delta < 2$ and disregarded the others as irrelevant since they led to stable scaling dimensions.

We observed from the $\alpha - \beta$ parameter space that there is a region of stability where the processes, CDW and SC, are RG irrelevant. The region of stability exists at any value of the relative coupling strength α from 0 to 1. We observed this in Fig. 10.1 where the product $K_{SC}/K_{CDW} > 1$. However, a weak modulation β causes an instability at small α. This can also indicate that disorder of inter-wire couplings can cause an instability of the SLL phase which is otherwise stable. At strong coupling for α close to 1 we found a considerably broad stability region within the $\alpha - \beta$ space. Correspondingly, the widest span of the values of the Luttinger parameter K ensuring stability is between $0.5 - 0.65$ for $\alpha = 1$ and $\beta = 0$.

11.3 Future work

This research could lead to many different avenues in the development of our understanding of topological materials and their unique properties. The next step would be to adapt our framework for the one-dimensional topological insulators to two-dimensions. The addition in dimensionality would change the model such that we would now have surface states, or edge states, unlike the previously exponentially decaying bound states. This generalisation to 2D would allow us to understand how the properties of reflection amplitudes relate to the presence or absence of edge states. As we know, topological insulators exist due to conducting surface states, so this generalisation would also allow us to identify a topological insulator.

Chapter 12

Bibliography

[1] M. Z. Hasan and C. L. Kane, "Colloquium: topological insulators," *Reviews of modern physics*, vol. 82, no. 4, p. 3045, 2010.

[2] S.-Q. Shen, *Topological insulators*, vol. 174. Springer, 2012.

[3] C. Han, M. Lee, S. Callard, C. Seassal, and H. Jeon, "Lasing at topological edge states in a photonic crystal l3 nanocavity dimer array," *Light: Science & Applications*, vol. 8, no. 1, pp. 1–10, 2019.

[4] S. A. Parameswaran and Y. Wan, "Topological insulators turn a corner," *Physics*, vol. 10, p. 132, 2017.

[5] Y. Ando, T. Hamasaki, T. Kurokawa, K. Ichiba, F. Yang, M. Novak, S. Sasaki, K. Segawa, Y. Ando, and M. Shiraishi, "Electrical detection of the spin polarization due to charge flow in the surface state of the topological insulator bi1. 5sb0. 5te1. 7se1. 3," *Nano letters*, vol. 14, no. 11, pp. 6226–6230, 2014.

[6] M. Franz and L. Molenkamp, *Topological insulators*. Elsevier, 2013.

[7] B. Mendelson, *Introduction to topology*. Courier Corporation, 1990.

[8] C. Li, S. Lin, G. Zhang, and Z. Song, "Topological nodal points in two coupled ssh chains," *arXiv preprint arXiv:1704.04990*, 2017.

[9] W. Su, J. Schrieffer, and A. J. Heeger, "Solitons in polyacetylene," *Physical review letters*, vol. 42, no. 25, p. 1698, 1979.

[10] P. Delplace, D. Ullmo, and G. Montambaux, "Zak phase and the existence of edge states in graphene," *Physical Review B*, vol. 84, no. 19, p. 195452, 2011.

[11] D. J. Thouless, M. Kohmoto, M. P. Nightingale, and M. den Nijs, "Quantized hall conductance in a two-dimensional periodic potential," *Physical review letters*, vol. 49, no. 6, p. 405, 1982.

[12] M. Kohmoto, "Topological invariant and the quantization of the hall conductance," *Annals of Physics*, vol. 160, no. 2, pp. 343–354, 1985.

[13] D. Tong, "Lectures on the quantum hall effect," *arXiv preprint arXiv:1606.06687*, 2016.

[14] A. Abrikosov, "Quantum magnetoresistance," *Physical Review B*, vol. 58, no. 5, p. 2788, 1998.

[15] W. Kim, L. Covaci, and F. Marsiglio, "Impurity scattering of wave packets on a lattice," *Physical Review B*, vol. 74, no. 20, p. 205120, 2006.

[16] L. Liang, S. Peotta, A. Harju, and P. Törmä, "Wave-packet dynamics of bogoliubov quasiparticles: Quantum metric effects," *Physical Review B*, vol. 96, no. 6, p. 064511, 2017.

[17] R. Robinett, M. Doncheski, and L. Bassett, "Simple examples of position-momentum correlated gaussian free-particle wave packets in one dimension with the general form of the time-dependent spread in position," *Foundations of Physics Letters*, vol. 18, no. 5, pp. 455–475, 2005.

[18] U. Klein, "What is the limit h to 0 of quantum theory?," *American Journal of Physics*, vol. 80, no. 11, pp. 1009–1016, 2012.

[19] S. Gasiorowicz, *Quantum physics*. John Wiley & Sons, 2007.

[20] D. J. Griffiths and D. F. Schroeter, *Introduction to quantum mechanics*. Cambridge University Press, 2018.

[21] G. Barton, "Levinson's theorem in one dimension: heuristics," *Journal of Physics A: Mathematical and General*, vol. 18, no. 3, p. 479, 1985.

[22] M. Bockrath, D. H. Cobden, J. Lu, A. G. Rinzler, R. E. Smalley, L. Balents, and P. L. McEuen, "Luttinger-liquid behaviour in carbon nanotubes," *Nature*, vol. 397, no. 6720, pp. 598–601, 1999.

[23] K. Schönhammer, "Luttinger liquids: the basic concepts," *Strong interactions in low dimensions*, pp. 93–136, 2004.

[24] N. T. Brönn, "Luttinger liquids," 2007.

[25] H. J. Schulz, G. Cuniberti, and P. Pieri, "Fermi liquids and luttinger liquids," in *Field theories for low-dimensional condensed matter systems*, pp. 9–81, Springer, 2000.

[26] T. Hansson, "Fermi and luttinger liquids," *Rev. Mod. Phys*, vol. 66, p. 129, 1994.

[27] J. Voit, "One-dimensional fermi liquids," *Reports on Progress in Physics*, vol. 58, no. 9, p. 977, 1995.

[28] D. Neilson, "Landau fermi liquid theory," *Australian journal of physics*, vol. 49, no. 1, pp. 79–102, 1996.

[29] S. Begum, V. Fleurov, V. Kagalovsky, and I. Yurkevich, "Sliding luttinger liquid with alternating interwire couplings," *Journal of Physics: Condensed Matter*, vol. 31, no. 42, p. 425601, 2019.

[30] V. Fleurov, V. Kagalovsky, I. V. Lerner, and I. V. Yurkevich, "Instability of the sliding luttinger liquid," *Journal of Physics: Condensed Matter*, vol. 30, no. 18, p. 185602, 2018.

[31] J. Morales, "Charge density waves: An emergent ground state in the manganites," *Paper, Department of Physics and Materials Research Laboratory, University of Illinois at Urbana-Champaign, Urbana, Illinois*, vol. 61801, 2009.

[32] A. Bianchi, R. Movshovich, N. Oeschler, P. Gegenwart, F. Steglich, J. Thompson, P. Pagliuso, and J. Sarrao, "First-order superconducting phase transition in c e c o i n 5," *Physical review letters*, vol. 89, no. 13, p. 137002, 2002.

[33] P. Collet *et al.*, "A renormalization group analysis of the hierarchical model in statistical mechanics," *A Renormalization Group Analysis of the Hierarchical Model in Statistical Mechanics*, 1978.

[34] Y. Hatsugai, "Chern number and edge states in the integer quantum hall effect," *Physical review letters*, vol. 71, no. 22, p. 3697, 1993.

[35] M. Gell-Mann and F. Low, "Bound states in quantum field theory," *Physical Review*, vol. 84, no. 2, p. 350, 1951.

[36] J. Singleton, *Band theory and electronic properties of solids*, vol. 2. Oxford University Press, 2001.

[37] E. Willett, *The basics of quantum physics: understanding the photoelectric effect and line spectra*. The Rosen Publishing Group, Inc, 2004.

[38] M. Massimi, *Pauli's exclusion principle: The origin and validation of a scientific principle*. Cambridge University Press, 2005.

[39] C. Kane and T. Lubensky, "Topological boundary modes in isostatic lattices," *Nature Physics*, vol. 10, no. 1, pp. 39–45, 2014.

[40] D. A. Bandurin, A. V. Tyurnina, L. Y. Geliang, A. Mishchenko, V. Zólyomi, S. V. Morozov, R. K. Kumar, R. V. Gorbachev, Z. R. Kudrynskyi, S. Pezzini, *et al.*, "High electron mobility, quantum hall effect and anomalous optical response in atomically thin inse," *Nature nanotechnology*, vol. 12, no. 3, pp. 223–227, 2017.

[41] A. Baumgartner, T. Ihn, K. Ensslin, G. Papp, F. Peeters, K. Maranowski, and A. Gossard, "Classical hall effect in scanning gate experiments," *Physical Review B*, vol. 74, no. 16, p. 165426, 2006.

[42] J. K. Asbóth, L. Oroszlány, and A. Pályi, "A short course on topological insulators," *Lecture notes in physics*, vol. 919, pp. 997–1000, 2016.

[43] R. Skomski and D. J. Sellmyer, "Nonadiabatic berry phase in nanocrystalline magnets," *AIP Advances*, vol. 7, no. 5, p. 055802, 2017.

[44] K. von Klitzing, "Essay: Quantum hall effect and the new international system of units," *Physical review letters*, vol. 122, no. 20, p. 200001, 2019.

[45] K. v. Klitzing, G. Dorda, and M. Pepper, "New method for high-accuracy determination of the fine-structure constant based on quantized hall resistance," *Physical review letters*, vol. 45, no. 6, p. 494, 1980.

[46] S. Hiyamizu, J. Saito, K. Nanbu, and T. Ishikawa, "Improved electron mobility higher than 106 cm2/vs in selectively doped gaas/n-algaas heterostructures grown by mbe," *Japanese journal of applied physics*, vol. 22, no. 10A, p. L609, 1983.

[47] D. Tsui, H. Störmer, and A. Gossard, "Zero-resistance state of two-dimensional electrons in a quantizing magnetic field," *Physical Review B*, vol. 25, no. 2, p. 1405, 1982.

[48] R. Laughlin, "Primitive and composite ground states in the fractional quantum hall effect," *Surface Science*, vol. 142, no. 1-3, pp. 163–172, 1984.

[49] B. A. Bernevig and S.-C. Zhang, "Quantum spin hall effect," *Physical review letters*, vol. 96, no. 10, p. 106802, 2006.

[50] I. Geru, *Time-reversal Symmetry: Seven Time-reversal Operators for Systems with Non-zero Angular... Momentum*. SPRINGER, 2019.

[51] S. A. H. Gangaraj, M. G. Silveirinha, and G. W. Hanson, "Berry phase, berry connection, and chern number for a continuum bianisotropic material from a classical electromagnetics perspective," *IEEE journal on multiscale and multiphysics computational techniques*, vol. 2, pp. 3–17, 2017.

[52] H. A. Priestley, *Introduction to complex analysis*. OUP Oxford, 2003.

[53] W. H. Young, *The fundamental theorems of the differential calculus*, vol. 11. The University Press, 1910.

[54] Y. Nambu, "Quasi-particles and gauge invariance in the theory of superconductivity," *Physical Review*, vol. 117, no. 3, p. 648, 1960.

[55] J. Von Delft and H. Schoeller, "Bosonization for beginners—refermionization for experts," *Annalen der Physik*, vol. 7, no. 4, pp. 225–305, 1998.

[56] C. Kane, "Lectures on bosonization," *Boulder Summer School lectures*, 2005.

[57] J. R. Taylor, *Scattering theory: the quantum theory of nonrelativistic collisions*. Courier Corporation, 2006.

[58] D. G. Duffy, *Green's functions with applications*. cRc press, 2015.

[59] L. Maiani and O. Benhar, *Relativistic Quantum Mechanics: An Introduction to Relativistic Quantum Fields*. CRC Press, 2015.

[60] J. E. Moore and L. Balents, "Topological invariants of time-reversal-invariant band structures," *Physical Review B*, vol. 75, no. 12, p. 121306, 2007.